

Heart failure potentially affects the cortical structure of the brain

Yinqin Hu^{1,*}, Tianyun Shi^{1,*}, Zhaohui Xu¹, Meng Zhang¹, Jiahui Yang¹, Zhirui Liu¹, Qiqi Wan¹, Yongming Liu^{1,2}

¹Department of Cardiovascular Disease, Shuguang Hospital Affiliated to Shanghai University of Traditional Chinese Medicine, Shanghai, China

²Anhui Provincial Hospital of Integrated Medicine, Anhui Hospital of Shuguang Hospital Affiliated to Shanghai University of TCM, Hefei 230011, Anhui, China

*Equal contribution

Correspondence to: Yongming Liu; **email:** liuyongming@foxmail.com, <https://orcid.org/0000-0002-1956-9534>

Keywords: psycho-cardiology, heart failure, cerebral cortex structure, Mendelian randomization, causal effect

Received: October 31, 2023

Accepted: March 25, 2024

Published: April 22, 2024

Copyright: © 2024 Hu et al. This is an open access article distributed under the terms of the [Creative Commons Attribution License](https://creativecommons.org/licenses/by/4.0/) (CC BY 4.0), which permits unrestricted use, distribution, and reproduction in any medium, provided the original author and source are credited.

ABSTRACT

Background: Heart failure (HF) has been reported to affect cerebral cortex structure, but the underlying cause has not been determined. This study used Mendelian randomization (MR) to reveal the causal relationship between HF and structural changes in the cerebral cortex.

Methods: HF was defined as the exposure variable, and cerebral cortex structure was defined as the outcome variable. Inverse-variance weighted (IVW), MR-Egger regression and weighted median (WME) were performed for MR analysis; MR-PRESSO and Egger's intercept was used to test horizontal pleiotropy; and "leave-one-out" was used for sensitivity analysis.

Results: Fifty-two single nucleotide polymorphisms (SNPs) were defined as instrumental variables (IVs), and there was no horizontal pleiotropy in the IVs. According to the IVW analysis, the OR and 95% CI of cerebral cortex thickness were 0.9932 (0.9868-1.00) (P=0.0402), and the MR-Egger intercept was -15.6×10^{-5} (P = 0.7974) and the Global test pval was 0.078. The P-value of the cerebral cortex surface was 0.2205, and the MR-Egger intercept was -34.69052 (P= 0.6984) and the Global Test pval was 0.045. HF had a causal effect on the surface area of the caudal middle frontal lobule (P=0.009), insula lobule (P=0.01), precuneus lobule (P=0.049) and superior parietal lobule (P=0.044).

Conclusions: HF was potentially associated with changes in cortical thickness and in the surface area of the caudal middle frontal lobule, insula lobule, precuneus lobule and superior parietal lobule.

INTRODUCTION

Heart failure (HF) is the severe or terminal stage of various heart diseases and is characterized by high morbidity, mortality, and hospitalization rates; poor quality of life; and high medical costs [1]. The data show that the global incidence of HF ranges from 1% to 3%. Due to population aging, the treatment and prognosis of ischemic heart disease have improved, and effective evidence-based treatment has prolonged the survival of patients with HF. However, the incidence of HF has continued to increase, ranging from 1/1000 person-years to 20/1000 person-years, and the prevalence in different

regional populations also differs. The incidence of HF in European and American populations ranges from 2/1000 person-years to 3/1000 person-years, and the incidence of HF is positively correlated with age [2]. Heart failure can lead to reduced pumping function of the heart muscle and reduced blood flow throughout the body, resulting in insufficient blood supply to the brain. In fact, abnormal cerebral hemodynamics may lead to a lack of glucose and oxygen in the brain, which in turn leads to a series of adverse biochemical events, ultimately leading to metabolic and tissue damage, which is a major cause of structural changes in the brain [3]. The structural changes in the cerebral cortex caused by this phenomenon are also

related mainly to cognitive dysfunction, such as vascular dementia and Alzheimer’s disease. Studies have shown that patients with coronary heart disease exhibit a wide range of gray matter density decreases, while patients with heart failure mainly exhibit a significant decrease in gray matter density in the posterior, middle and precuneus regions of the cingulate gyrus [4]. Moreover, the cortical thickness of the frontal, parietal, temporal and occipital lobes is reduced in patients with heart failure, which mainly controls autonomic, cognitive, emotional, language and visual functions. With the atrophy of these functional cortical areas, patients also exhibit corresponding neurological dysfunction [5]. Brain structure is closely related to heart failure, and the existing research is limited mainly to the study of brain structure changes caused by hemodynamics; however, there is no clear targeted research on whether there is a genetic link between heart failure and cerebral cortex structure.

Randomized controlled trials (RCTs) are not implemented clinically due to various limiting factors, and observational experimental methods can lead to biased study results due to confounding factors and reverse causation, resulting in relatively low credibility. Mendelian randomization (MR) involves an analysis of genetic variables that follow Mendel’s law of inheritance and exploits single nucleotide polymorphisms (SNPs) as instrumental variables (IVs) to infer the causality of an observed association between a modifiable exposure and a clinically relevant outcome [6]. Alleles are randomly separated during meiosis, so MR can reduce the bias caused by confounding factors [7]. In addition, since genetic variation occurs before disease and the order of the two cannot be reversed, MR can also avoid the interference of reverse causality [7].

This study was based on a large sample genome-wide association study (GWAS; GE-Nanowide Association

Study). SNP sites published in the GWAS database were used as instrumental variables of genetic variation to explore the causal relationship between HF and cerebral cortex structure through a two-sample MR research method.

MATERIALS AND METHODS

Study design

In this study, heart failure was used as an exposure factor, and single nucleotide polymorphisms (SNPs) that were significantly correlated with heart failure were used as instrumental variables (IVs). The cerebral cortex structure was selected as the outcome. The TwoSampleMR package in R was used to conduct causal association analysis, and the Cochran Q heterogeneity test, pleiotropy test and sensitivity analysis were performed to verify the reliability of the results. MR analysis relies on three assumptions, as shown in Figure 1 [8]: (1) IVs are strongly correlated with exposure variables, (2) IVs are not associated with confounding factors affecting exposure outcomes, and (3) IVs affect outcome factors only through exposure factors.

Data sources

We searched for GWAS data on HFs and the cerebral cortex on the website ‘<https://gwas.mrcieu.ac.uk/datasets>’. The data for HF (ebi-a-GCST009541) were derived from the GWAS statistical results published in 2020 and included a sample of 977,323 people, 47,309 cases and 930,014 controls, and 7,773,021 SNPs. In this study, GWAS data related to cortical structure were obtained from the ENIGMA study, a genome-wide association meta-analysis of brain magnetic resonance imaging data from 51,665 people; the surface area, average

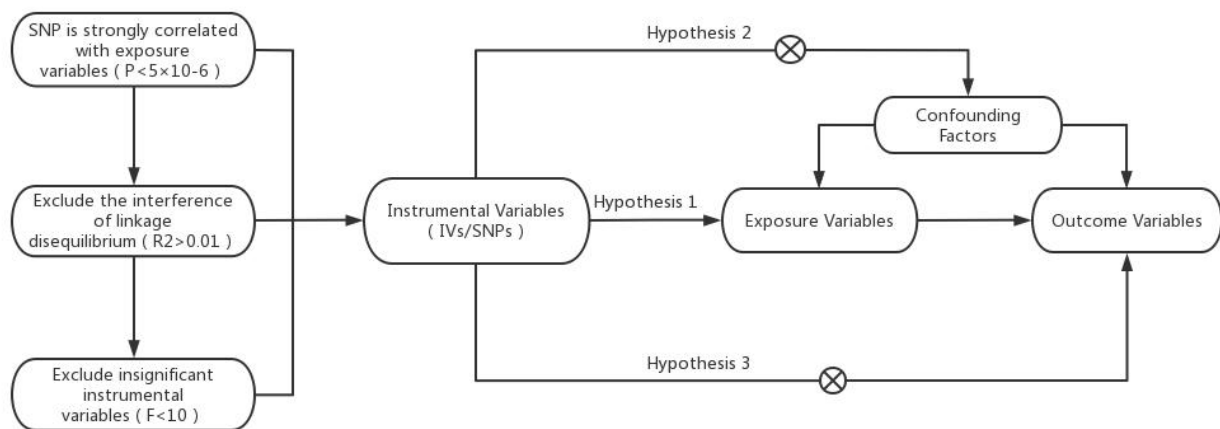


Figure 1. Model of the Mendelian randomization analysis.

thickness, and 34 known functional regions of the entire cortex were analyzed. The HF patients with cerebral cortex structure data included in this study were mostly European.

Instrumental variables

We obtained HF-related genetic data from the website '<https://gwas.mrcieu.ac.uk/datasets>' using R software. To avoid analytical bias caused by linkage disequilibrium (LD) between SNPs, we used all SNPs that were significant ($P < 5 \times 10^{-8}$) and predicted significant genome-wide exposure. SNPs with an R^2 value >0.001 and a base physical distance less than 10,000 kb were removed, and SNPs with the smallest P-values were retained. Candidate SNPs were matched with GWAS data for the outcome variable based on the chromosome and location. To further evaluate weak IV bias, the F statistic was used to calculate the power of the IV. When the IVs with an F value <10 were eliminated, the specific calculation formula was $F = \beta^2 / SE^2$, where β^2 is the effect value of the β allele and SE is the standard error. Since only 12 significant and independent SNPs with genome-wide significance remained after screening, we used a higher P-value ($P < 5 \times 10^{-6}$) to obtain SNPs predicting HF as the final IV included in the study.

MR and sensitivity analysis

The analysis methods used in this study were mainly the inverse-variance weighted (IVW) method in the TwoSampleMR package [9, 10], MR-Egger regression [11] and the weighted median (WME) method [12].

The heterogeneity test tests the difference between various IVs. If P was >0.05 , there was no heterogeneity. In this study, the P -value of the Cochran Q test was used to assess heterogeneity. A P -value <0.05 indicated heterogeneity. In contrast, $P > 0.05$ indicated no heterogeneity. The pleiotropy test [13] verifies the reliability of MR analysis results and is often performed via the MR-PRESSO test and the intercept term of the MR-Egger regression method. $P > 0.05$ was considered to indicate no horizontal pleiotropy; if pleiotropy was indicated, the MR analysis results were not reliable. The "leave-one-out" method [14] was adopted to test the sensitivity. The principle is to gradually eliminate the results of a single SNP to determine whether the results are outliers and to observe the stability and reliability of the results after the removal of each SNP.

Availability of data and materials

All data are publicly available.

Consent for publication

Written informed consent for publication was obtained from all participants.

RESULTS

Instrumental variables

In this study, HF was taken as an exposure factor, R software was used to screen SNPs with genome-wide significance according to the screening criteria, and a total of 52 SNPs were included as IVs. Table 1 shows the 15 most significant SNPs, and the remaining complete SNP data are shown in Supplementary Table 1.

MR analysis of HF and cortical thickness

In this study, IVW regression, MR-Egger regression and WME analysis in the TwoSampleMR package were used to perform MR analysis of HF and cerebral cortex thickness. Table 2 shows the results of the MR analysis, and the scatter plot is shown in Figure 2. IVW analysis revealed $\beta = -0.0068$, $SE = 0.0033$, $P = 0.0402$ and an OR ($95\% CI$) = 0.9932 (0.9868-1.00); MR-Egger analysis revealed $\beta = -0.004$, $SE = 0.0114$, $P = 0.7273$, and an OR ($95\% CI$) = 0.996 (0.974-1.0185). WME analysis revealed $\beta = -0.005$, $SE = 0.0041$, $P = 0.2223$, and OR ($95\% CI$) = 0.995 (0.9871-1.003). Although the results of the MR-Egger and WME analyses showed that HF had no significant effect on the thickness of the cerebral cortex, the results of the IVW analysis showed $P = 0.0402$. In addition, the β values of the IVW, MR-Egger and WME analyses were in the same direction, and the IVW results prevailed. Moreover, we used the MR-Egger intercept to verify the presence of pleiotropy in this study. The results showed an Egger's intercept value of -15.6×10^{-5} , which is infinitely close to 0, $SE = 6.04 \times 10^{-4}$, $P = 0.7974$ and the global test $pval = 0.078$, indicating that horizontal pleiotropy did not exist. There was no multi-effect interference in the MR results. Therefore, these results suggest that HF has a significant effect on the thickness of the cerebral cortex, that there is a causal relationship between the two, and that the thickness of the cerebral cortex is negatively correlated with the incidence of HF.

MR analysis of the HF and cortical surface

In this study, IVW, MR-Egger regression and WME analyses in the TwoSampleMR package were used to perform MR analysis of HFs and the surface area of the cerebral cortex. Table 3 shows the results of the MR analysis, and the scatter plot is shown in Figure 3. IVW analysis revealed $\beta = -601.7768$, $SE = 491.1655$, $P = 0.2205$, and OR ($95\% CI$) = 4.483756E-262 (0-5.497039E +156);

Table 1. Basic information of the SNPs associated with HF.

SNPs	CHR	POS	Other allele	Effect allele	β	SE	P
rs55751848	1	57018257	C	G	-0.0425	0.0089	1.79E-06
rs593467	1	70584460	G	A	-0.0548	0.0118	3.42E-06
rs660240	1	109817838	T	C	0.0611	0.0097	3.00E-10
rs35054810	1	222722282	G	A	0.0725	0.0143	3.98E-07
rs7559452	2	3885011	A	G	0.0468	0.0102	4.47E-06
rs17496249	2	37102249	A	G	-0.0372	0.0079	2.49E-06
rs12477245	2	107584422	C	T	0.1192	0.0236	4.40E-07
rs7369998	2	125815568	G	A	-0.059	0.0126	2.83E-06
rs72844714	2	133386122	C	A	0.0559	0.0121	3.84E-06
rs80087882	2	201379864	G	A	0.0609	0.0125	1.10E-06
rs4376020	3	5397743	T	A	-0.0612	0.0123	6.50E-07
rs9815816	3	85930582	T	C	0.0479	0.0099	1.31E-06
rs10938398	4	45186139	G	A	0.0389	0.008	1.16E-06
rs11722972	4	69897984	T	G	-0.0519	0.0114	5.30E-06
rs2634071	4	111669220	T	C	-0.0923	0.0101	6.33E-20

SNPs, single nucleotide polymorphisms; CHR, chromosome; POS, location; EA, effector allele; OA, noneffector allele. β , standard error. SE, standard error of beta.

Table 2. MR results of cortical thickness in HF patients.

MR method	β	SE	OR (95% CI)	P
IVW	-0.0068	0.0033	0.9932 (0.9868-1.00)	0.0402
MR-Egger	-0.004	0.0114	0.9960 (0.974-1.0185)	0.7273
Weighted median	-0.005	0.0041	0.995 (0.9871-1.003)	0.2223

MR, Mendelian randomization; β , beta; SE, standard error; OR, odds ratio; IVW, inverse-variance weighted.

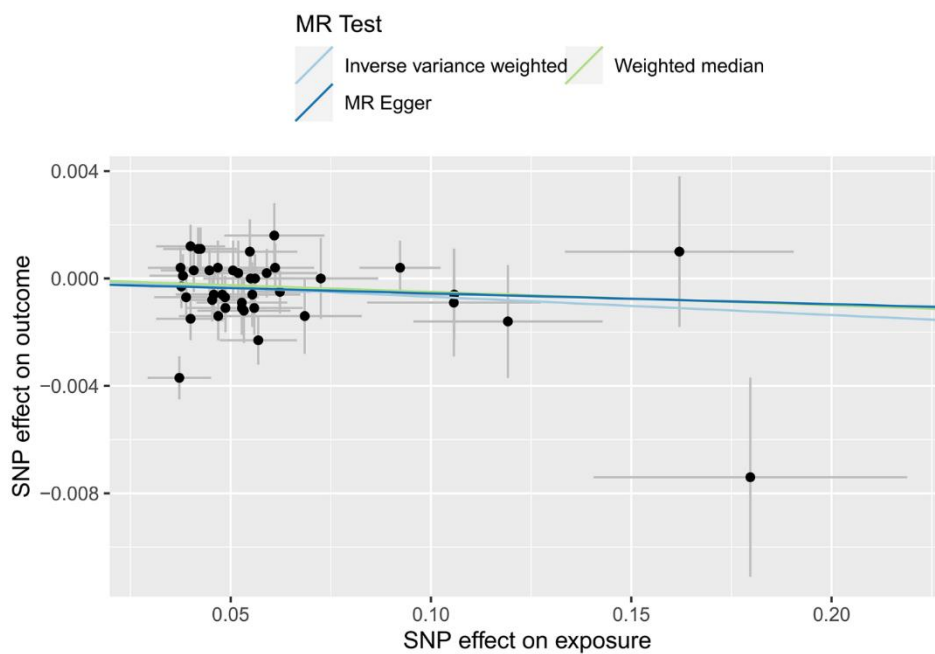


Figure 2. MR scatter plot of cortical thickness in HF patients.

Table 3. MR results of the effect of HF on cortical surface area.

MR method	β	SE	OR (95% CI)	P
IVW	-601.7768	491.1655	4.483756E-262 (0-5.497039e+156)	0.2205
MR-Egger	23.0309	1675.8267	1.005105e+10 (0-inf)	0.9891
Weighted median	-535.222	641.9665	3.597802E-233 (0-inf)	0.4044

MR, Mendelian randomization; β , beta; SE, standard error; OR, odds ratio; IVW, inverse-variance weighted.

MR-Egger analysis revealed $\beta=23.0309$, $SE=1675.8267$, $P=0.9891$, and $OR (95\% CI)=1.005105e+10 (0-inf)$; and WME analysis showed $\beta=-535.222$, $SE=641.9665$, $P=0.4044$, and $OR (95\% CI)=3.597802E-233 (0-inf)$. According to the results of the IVW, MR-Egger and WME analyses, none of the three analysis methods showed statistical significance, suggesting that there was no direct causal relationship between the cerebral cortex surface area and HF incidence. Moreover, we used the MR-Egger intercept to verify the presence of pleiotropy in this study, and the results showed Egger's intercept=-34.69052, $SE = 88.86852$, $P = 0.6984$, and a global test $pval=0.045$, indicating that heart failure and cerebral cortex surface area may be pleiotropic.

MR analysis of the HF and cerebral cortex

In this study, according to 34 specific cerebral cortical functional areas with known functions defined by the Desikan-Killiany atlas [15], the IVW analysis

method in the TwoSampleMR package was used to conduct MR analysis on the effects of HF on the structure of cerebral cortical functional areas. In this section, we present the MR analysis results for 34 functional brain regions using the global weighted method because the global weighted method may be less affected by neuroanatomical variation between different individuals [16]. Figure 4 and Supplementary Table 2 show the results of this part of the study, suggesting that HF had a significant impact on the surface area of the caudal middle frontal lobule ($P=0.009$), insula lobule ($P=0.01$), precuneus lobule ($P=0.049$) and thickness of the superior parietal lobule ($P=0.044$). This difference was statistically significant. A scatter diagram of the MR analysis of the structure of various functional areas of the cerebral cortex in HF patients is shown (Supplementary Figures 1–3, 8–10). The pleiotropic analysis of the effects of HF on the structure of various functional areas of the brain is shown in Supplementary Tables 3, 4.

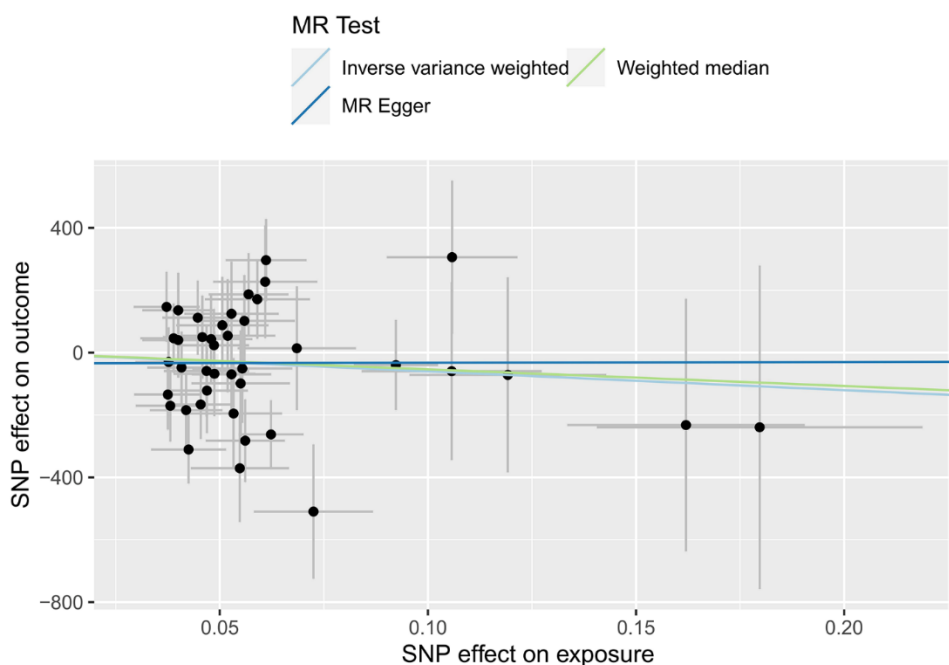


Figure 3. MR scatter plot of the effect of HF on the cerebral cortex surface area.

Sensitivity analysis of the HF and cerebral cortex structure

This study strictly followed the screening criteria for IVs, and most of the included participants were European; therefore, the possibility of false negative results was unlikely, and the results were tested for heterogeneity. The IVW test of the effect of HF on cerebral cortex thickness yielded Cochran’s $Q=53.8265$ and $P=0.071$; the MR–Egger test yielded Cochran’s $Q=53.7344$ and $P=0.058$. All P -values were >0.05 , indicating no heterogeneity. The results are shown in Figure 5.

The IVW test of the effect of HF on the cerebral cortex surface area yielded Cochran’s $Q=56.6142$ and $P=0.042$; the MR–Egger test yielded Cochran’s $Q=56.3939$ and $P=0.035$. All P -values were <0.05 , indicating heterogeneity. The results are shown in Figure 6. A funnel plot for the analysis of cortical heterogeneity in the relationship between various functional areas of the brain and HF is shown in Supplementary Figures 4, 5, 11, 12 and Supplementary Tables 5, 6.

Subsequently, we applied the “leave-one-out” method of sensitivity analysis to visualize the IVW analysis results of the relationship between HF and cerebral

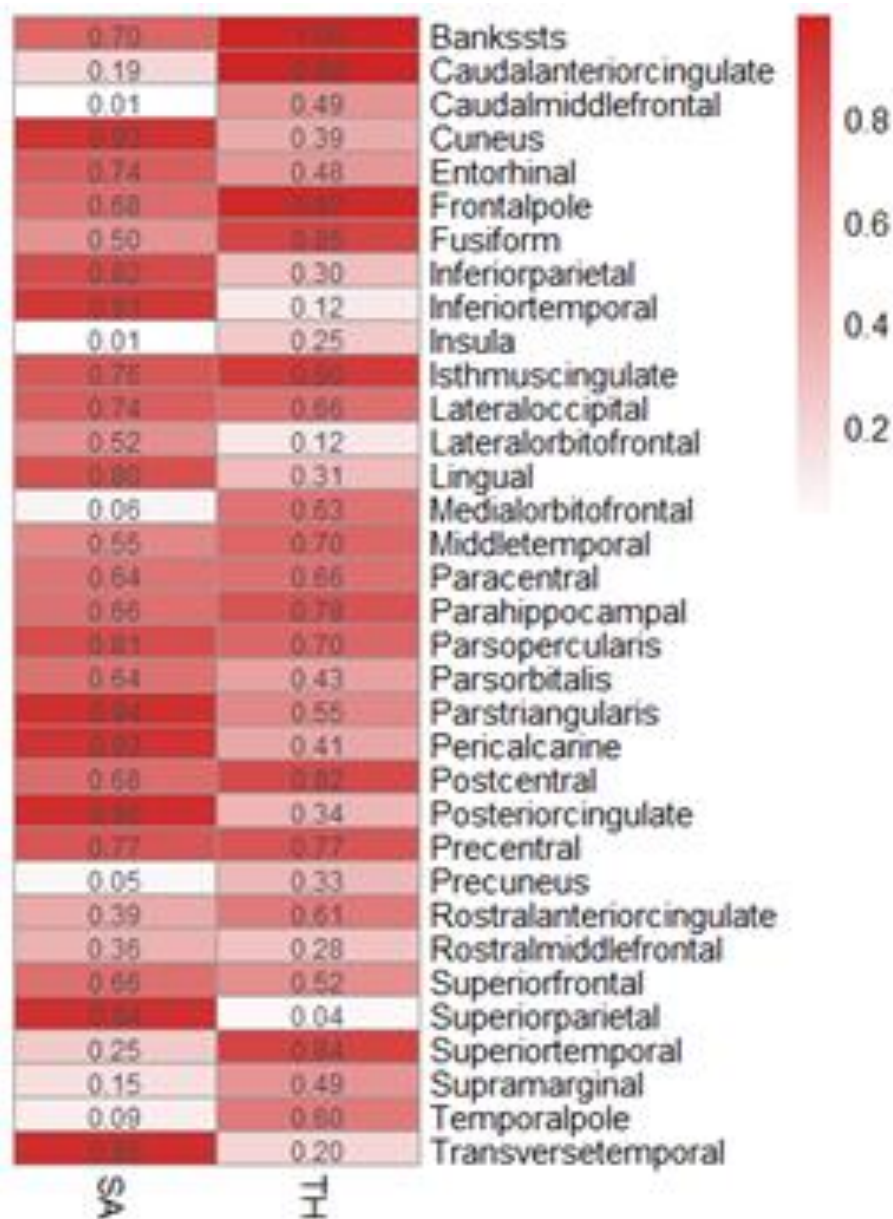


Figure 4. MR heatmap of the effect of HF on the structure of the cerebral cortex.

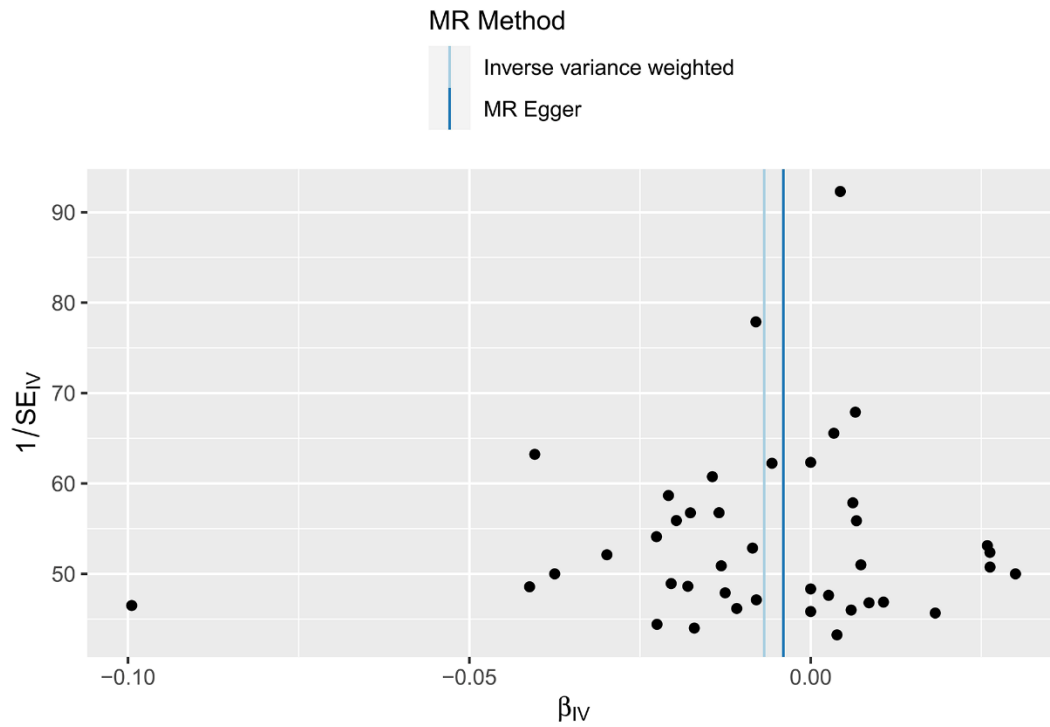


Figure 5. Funnel plot of the heterogeneity test results for the effect of HF on cerebral cortex thickness according to the MR method.

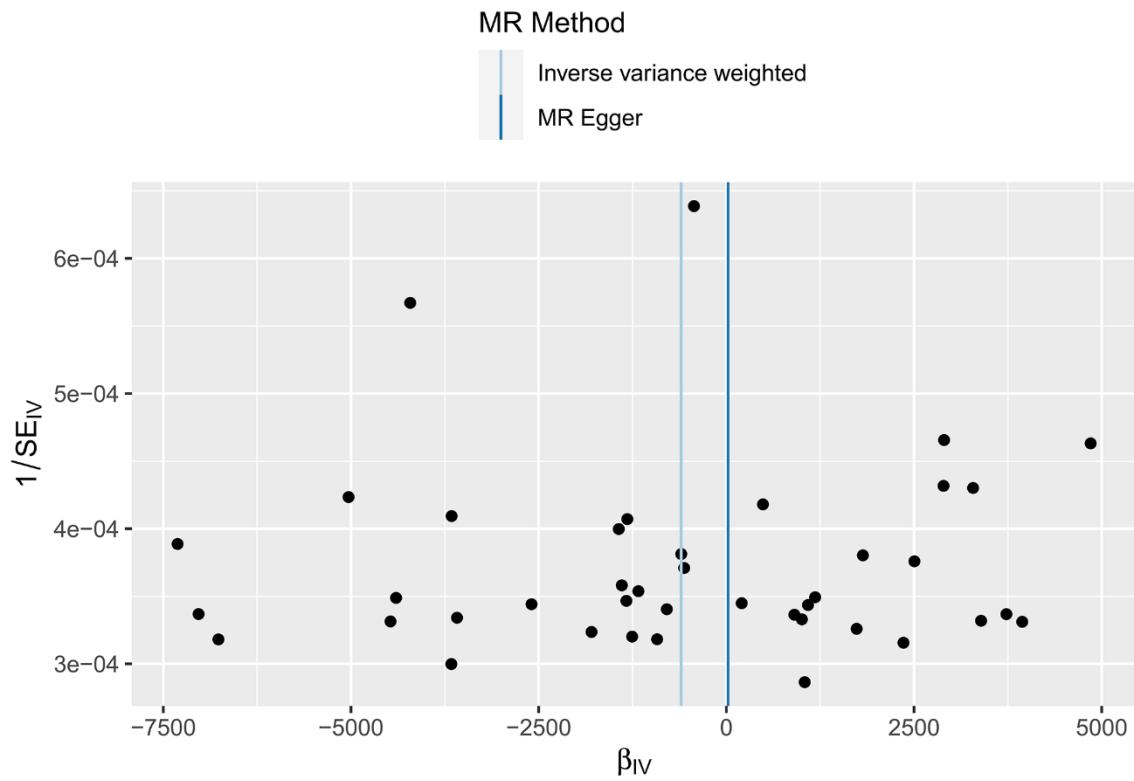


Figure 6. Funnel plot of the heterogeneity test results of the MR analysis of the relationship between HF and the cerebral cortex surface area.

cortex structure (Figures 7, 8). After the above significant and independent SNPs were sequentially excluded, the IVW outcome effect values of the remaining SNPs did not significantly fluctuate. All the SNPs were close to the red dot position in the forest plot, and all the *P*-values were >0.05 , indicating that there was no SNP in the IVs that strongly influenced the results; this finding showed that the results obtained by the IVW analysis method were stable and reliable. The sensitivity analysis results of the effects of HF on the various functional areas of the brain are shown in Supplementary Figures 6, 7, 13, 14.

DISCUSSION

At present, numerous observational studies have shown that cerebral cortex structure is related to HF incidence, but there is no evidence showing whether there is a causal relationship between the two conditions. This study systematically identified a causal relationship between HF and cerebral cortex structure using two-sample MR analysis. Our findings suggest that HF affects cortical thickness, specifically the surface area of the caudal middle frontal lobule, insula, precuneus lobule, and superior parietal lobule. Moreover, sensitivity analysis did not reveal pleiotropy, further confirming the stability of the conclusion. This difference may be related to the reduced pumping function of the heart muscle in patients with HF.

Cortical structure, specifically cortical thickness, is considered a neuroimaging biomarker for predicting cognitive decline. Moreover, it is also believed that the surface area of the cerebral cortex is the key to reducing cortical volume in patients with cognitive or mental disorders [17]. Moreover, numerous studies have suggested that cortical surface area may be more sensitive than cortical thickness for the prediction of mental illness [18–20]. The middle frontal gyrus, where the caudal middle frontal lobule is located, is a region of the ventral prefrontal cortex that has been recognized as an important brain region leading to depression and is responsible for many cognitive functions. Examples of emotion processing include decision processing, emotional cognition [21], working memory [22], attention processing [23, 24], and top-down regulation in emotional processing [25]. Moreover, the prefrontal regions (BA8, BA9, BA10, BA46, and BA47), where the medial frontal gyrus is located, are located in front of the motor and premotor areas. These functional areas are related to human personality and determine a person's social and moral consciousness and emotional depth [26].

The insula, located deep in the lateral sulci of the brain, is also known as the “Island of Reil” and is

located deep in the temporal lobe. The insula was originally described as the paralimbic or limbic integration cortex [27]. Analysis of nearly 1,800 functional neuroimaging experiments revealed that the insula is divided into four main functional regions: the sensorimotor, central-olfactogustatory, socioemotional and cognitive anterior-dorsal regions [28]. The anterior insula, as the cortical center for visceral information processing and perception, is believed to play a crucial role in emotional experiences and subjective feelings [29]. Neural function imaging has shown that the expression of negative emotions is also related to the activation of the insula [30]. Moreover, patients with insular lobe injury exhibit various changes in subjective emotions, mainly manifested as anxiety-related indifference [31, 32]. The insula may play an important role in the management of social emotions.

The precuneus is a functional region of the parietal lobe; as one of the core regions of the default network, the precuneus is involved in the human body's situational memory, self-focused attention, visuospatial intention and self-emotional processing [33]. We found that the functional connectivity of the Brodmann region 47/12 of the lateral orbitofrontal cortex was enhanced with the precuneus, angular gyrus and Brodmann region 21 of the visual cortex. This enhanced nonreward or punishment system (Brodmann: BA47 and areas 12) with functional connections to the precuneus and angular gyrus is associated with explicit emotional negative self-awareness and self-esteem in individuals with depression [34]. The posterior cingulate cortex and anterior cuneus are considered hubs of the default mode network (DMN) and are involved in social cognition and theory of mind. Moreover, a previous study revealed that the functional connectivity of the posterior cingulate gyrus, anterior cuneus and angular gyrus is related to the severity of depression [35]. In addition, studies have shown that the superior lobular cortex plays an important role in cognitive control and detail attention [36, 37].

Subsequently, we analyzed the SNPs significantly associated with heart failure identified in the present study and observed that the expression of GPR39 corresponding to rs72844714 decreased in the hippocampus and cortex of patients with depression [38]. Zinc, a stimulator of GPR39, can activate the *G*α pathway, leading to an increase in cyclic adenosine monophosphate (cAMP) and activation of protein kinase A (PKA). This pathway can result in phosphorylation of cAMP response element-binding protein (CREB) and an increase in cAMP response element (CRE)-dependent transcription. Consequently, BDNF leads to the upregulation of brain-derived neurotrophic factor (BDNF) and tropomyosin receptor kinase B (TrkB) in

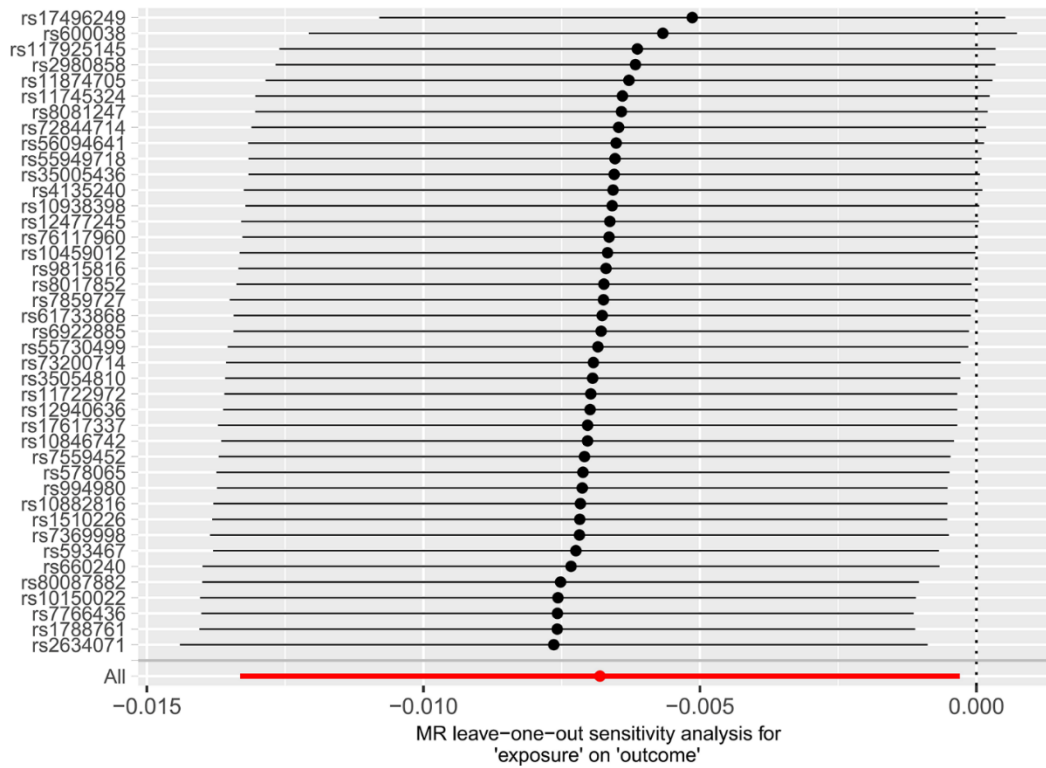


Figure 7. Forest plot of the “leave-one-out” method in the MR analysis of the relationship between HF and cerebral cortex thickness.

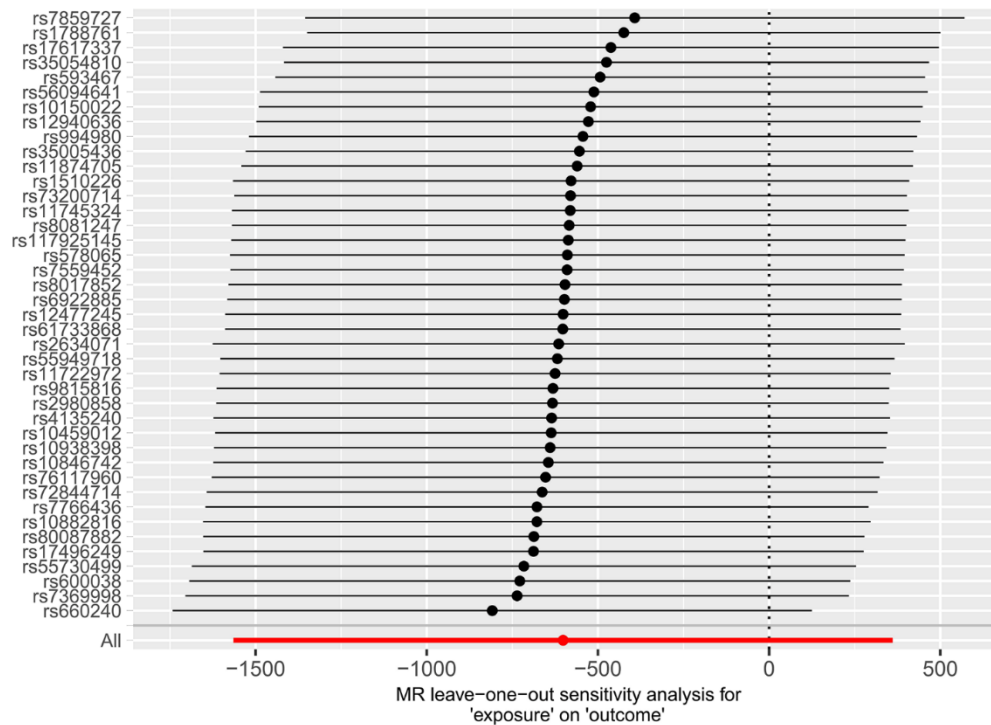


Figure 8. Forest plot of the “leave-one-out” method used in the MR analysis of the relationship between HF and cerebral cortex surface area.

neurons [39]. A zinc-deficient diet for 6 weeks can reduce the protein expression of GPR39 and BDNF in the prefrontal cortex [40]. After prolonged antidepressant treatment, GPR39 is upregulated, where it exerts antidepressant effects through the $G\alpha_q$ pathway via the CREB/BDNF/TrkB pathway [41–43]. Simultaneously, zinc can activate postsynaptic GPR39-mediated increases in intracellular calcium [44]. Calcium release, through upregulation of the postsynaptic membrane KCC2 (K⁺/Cl⁻) cotransporter protein, increases K-dependent Cl⁻ efflux in postsynaptic cells, thereby enhancing inhibitory tone and preventing excitotoxicity [44–46].

Notably, GPR39 is closely associated with the dopaminergic and 5-HT systems. When mice are treated with tyrosine hydroxylase inhibitor (alphaMT) and tryptophan hydroxylase inhibitor (pCPA) to block dopamine and 5-HT synthesis, GPR39 in the prefrontal cortex is significantly upregulated [47, 48]. Furthermore, the striatin (STRN) gene corresponding to rs17496249 is widely expressed in the striatum and serves as a regulator of striatal neuron development; moreover, this gene is significantly relevant for diagnosing symptomatic depression in patients with subsyndromal syndromes and severe depressive disorders [50, 51]. The FTO gene corresponding to rs56094641 is highly enriched in the cortex and hippocampus. Interaction with CaMKII delays the dephosphorylation of CREB in human neuroblastoma cells [52]. CaMKII-mediated activation of CREB promotes the transcription and translation

of the key neuronal plasticity proteins SYN and PSD95 [53, 54], potentially influencing the occurrence of depression. Further research has confirmed the neuroprotective role of hippocampal FTO in depression-like behavior through the activation of the CaMKII/CREB signaling pathway, improving hippocampal synaptic plasticity (dendritic remodeling, PSD95, and SYN expression) [55].

The structural changes in the cerebral cortex caused by HF may lead to a range of neuropsychiatric symptoms in patients. The link between psychosocial factors and CVD incidence has been identified as an important public health problem that mainly includes psychiatric symptoms such as anxiety and depression and can increase the occurrence of major adverse cardiovascular events [56]. Depression and anxiety have been shown to be prevalent in approximately 15%-20% of CVD patients and can coexist for a long time [57]. This, together with the results of this study, also confirms the theory of “psycho-cardiology”. The concept of “psycho-cardiology” began with an article published in the American Journal of Psychosomatics in 1985 titled “Psychocardiology: meeting place of the heart and mind” [58]. Therefore, we suggest that timely and appropriate mental health education and treatment should be given to patients with HF and other heart diseases to reduce the incidence of various psychiatric symptoms and improve the prognosis of patients with CVD.

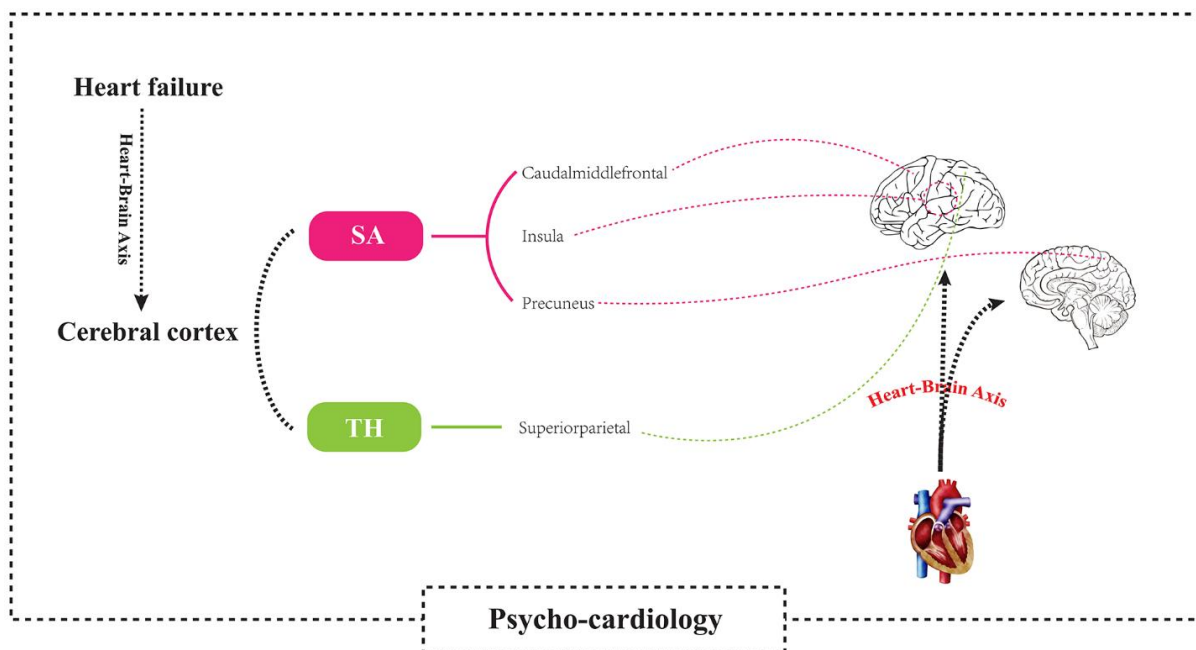


Figure 9. Using a two-sample Mendelian randomization framework, we revealed that heart failure causally influences brain cortical structure alterations, supporting the existence of the “heart-brain axis”. SA, Surface area; TH, thickness.

This study explored the effect of HF on cerebral cortex structure at the genetic level. According to our review results, this study is the first to perform MR analysis on the causal relationship between HF and cerebral cortex structure. Our results showed that although there was a direct effect of HF only on the cortical thickness of the whole-brain structure, there was a direct causal relationship between HF and the surface areas of the caudal middle frontal lobule, insula lobule, and precuneus lobule and the cortical thickness of the superior parietal lobule. This result supports the causal relationship between cardiac injury and neurological dysfunction, providing systematic and strong evidence for the theory of the “heart-brain axis” and “psycho-cardiology” Figure 9.

This study has several limitations. First, our study was limited to individuals of European descent, so whether our findings are generalizable to other individuals of different ethnicities remains unknown. Second, in this two-sample MR study design, we were unable to determine whether there was sample overlap between the exposure and outcome factor populations of the included GWAS dataset, which could lead to bias in the results. Third, we did not distinguish the phenotypes of patients with HF in more detail, such as those with reserved ejection fraction, those with reduced ejection fraction, or those with intermediate ejection fraction; therefore, we did not explore the effects of these different phenotypes on cerebral cortex structure. Finally, although a series of methods were used to rule out potential confounders and outliers and the sensitivity analyses did not detect any pleiotropy, we still cannot completely rule out all potential pleiotropy. Given these limitations, additional research should be performed to better confirm these possible associations, especially the clinical outcomes reflected in these results.

CONCLUSIONS

In summary, this study revealed a direct association between HF and cerebral cortex structure through comprehensive and systematic MR analysis. Our results showed that the surface area of the caudal middle frontal lobule, insula lobule, and precuneus lobule and the cortical thickness of the superior parietal lobule were directly affected by HF. Head MRI may be used for the early diagnosis and prediction of neuropsychiatric diseases in patients with HF. To some extent, this study provides a theoretical basis for theories of the “heart-brain axis” and “psycho-cardiology”. However, due to the limitations of this study, the specific mechanism of the “heart-brain axis” should be further investigated.

AUTHOR CONTRIBUTIONS

Hu Y.Q. designed the study, wrote the first draft of the manuscript and verified the underlying data. Hu Y.Q., Xu Z.H., Yang J.H. conducted the statistical analysis, Xu Z.H., Zhang M. and Shi T.Y. played a role in the acquisition of the data and analyses, and participated in data interpretation. Liu Z.R. and Wan Q.Q edited the figures and tables. Liu Y.M. directed the study design and funded the study. All authors revised and approved the final manuscript. The guarantor (Liu Y.M.) confirms that all listed authors meet the authorship criteria and that no others meeting the criteria have been omitted.

ACKNOWLEDGMENTS

We would like to extend our sincere gratitude to the corresponding author of this study, Yongming Liu, for her instructive advice and useful suggestions on this study. We are deeply grateful of her funding and help in the completion of this study.

CONFLICTS OF INTEREST

All authors declare the following: no support from any organization for the submitted work; no financial relationships with any organizations that might have an interest in the submitted work in the previous three years; and no other relationships or activities that could appear to have influenced the submitted work.

FUNDING

This study was supported by the National Natural Science Foundation of China (No. 81973611) and the Traditional Chinese Medicine Advantage Disease Diagnosis and Treatment Capacity Construction Project of Administration of Traditional Chinese Medicine of Anhui Province (340000232428000100010).

REFERENCES

1. Benjamin EJ, Muntner P, Alonso A, Bittencourt MS, Callaway CW, Carson AP, Chamberlain AM, Chang AR, Cheng S, Das SR, Delling FN, Djousse L, Elkind MS, et al, and American Heart Association Council on Epidemiology and Prevention Statistics Committee and Stroke Statistics Subcommittee. Heart Disease and Stroke Statistics-2019 Update: A Report From the American Heart Association. *Circulation*. 2019; 139:e56–528.
<https://doi.org/10.1161/CIR.0000000000000659>
PMID:[30700139](https://pubmed.ncbi.nlm.nih.gov/30700139/)
2. Lampros P, Prabhjot G, Andreas PK, Kalogeropoulos AP, Skopicki HA, Butler J. *Heart Failure: An Essential Clinical Guide*. 1st ed. Boca Raton: CRC Press. 2022:244–53.

3. Zhao Y, Gong CX. From chronic cerebral hypoperfusion to Alzheimer-like brain pathology and neurodegeneration. *Cell Mol Neurobiol.* 2015; 35:101–10.
<https://doi.org/10.1007/s10571-014-0127-9>
PMID:[25352419](https://pubmed.ncbi.nlm.nih.gov/25352419/)
4. Mueller K, Thiel F, Beutner F, Teren A, Frisch S, Ballarini T, Möller HE, Ihle K, Thiery J, Schuler G, Villringer A, Schroeter ML. Brain Damage With Heart Failure: Cardiac Biomarker Alterations and Gray Matter Decline. *Circ Res.* 2020; 126:750–64.
<https://doi.org/10.1161/CIRCRESAHA.119.315813>
PMID:[31969053](https://pubmed.ncbi.nlm.nih.gov/31969053/)
5. Kumar R, Yadav SK, Palomares JA, Park B, Joshi SH, Ogren JA, Macey PM, Fonarow GC, Harper RM, Woo MA. Reduced regional brain cortical thickness in patients with heart failure. *PLoS One.* 2015; 10:e0126595.
<https://doi.org/10.1371/journal.pone.0126595>
PMID:[25962164](https://pubmed.ncbi.nlm.nih.gov/25962164/)
6. Holmes MV, Ala-Korpela M, Smith GD. Mendelian randomization in cardiometabolic disease: challenges in evaluating causality. *Nat Rev Cardiol.* 2017; 14:577–90.
<https://doi.org/10.1038/nrcardio.2017.78>
PMID:[28569269](https://pubmed.ncbi.nlm.nih.gov/28569269/)
7. Zheng J, Baird D, Borges MC, Bowden J, Hemani G, Haycock P, Evans DM, Smith GD. Recent Developments in Mendelian Randomization Studies. *Curr Epidemiol Rep.* 2017; 4:330–45.
<https://doi.org/10.1007/s40471-017-0128-6>
PMID:[29226067](https://pubmed.ncbi.nlm.nih.gov/29226067/)
8. Hemani G, Zheng J, Elsworth B, Wade KH, Haberland V, Baird D, Laurin C, Burgess S, Bowden J, Langdon R, Tan VY, Yarmolinsky J, Shihab HA, et al. The MR-Base platform supports systematic causal inference across the human phenome. *Elife.* 2018; 7:e34408.
<https://doi.org/10.7554/elife.34408> PMID:[29846171](https://pubmed.ncbi.nlm.nih.gov/29846171/)
9. Wu F, Huang Y, Hu J, Shao Z. Mendelian randomization study of inflammatory bowel disease and bone mineral density. *BMC Med.* 2020; 18:312.
<https://doi.org/10.1186/s12916-020-01778-5>
PMID:[33167994](https://pubmed.ncbi.nlm.nih.gov/33167994/)
10. Yuan S, Larsson S. Causal associations of iron status with gout and rheumatoid arthritis, but not with inflammatory bowel disease. *Clin Nutr.* 2020; 39:3119–24.
<https://doi.org/10.1016/j.clnu.2020.01.019>
PMID:[32044136](https://pubmed.ncbi.nlm.nih.gov/32044136/)
11. Burgess S, Thompson SG. Interpreting findings from Mendelian randomization using the MR-Egger method. *Eur J Epidemiol.* 2017; 32:377–89.
<https://doi.org/10.1007/s10654-017-0255-x>
PMID:[28527048](https://pubmed.ncbi.nlm.nih.gov/28527048/)
12. Bowden J, Davey Smith G, Haycock PC, Burgess S. Consistent Estimation in Mendelian Randomization with Some Invalid Instruments Using a Weighted Median Estimator. *Genet Epidemiol.* 2016; 40:304–14.
<https://doi.org/10.1002/gepi.21965> PMID:[27061298](https://pubmed.ncbi.nlm.nih.gov/27061298/)
13. Carter AR, Sanderson E, Hammerton G, Richmond RC, Davey Smith G, Heron J, Taylor AE, Davies NM, Howe LD. Mendelian randomisation for mediation analysis: current methods and challenges for implementation. *Eur J Epidemiol.* 2021; 36:465–78.
<https://doi.org/10.1007/s10654-021-00757-1>
PMID:[33961203](https://pubmed.ncbi.nlm.nih.gov/33961203/)
14. Shi Y, Feng S, Yan M, Wei S, Yang K, Feng Y. Inflammatory bowel disease and celiac disease: A bidirectional Mendelian randomization study. *Front Genet.* 2022; 13:928944.
<https://doi.org/10.3389/fgene.2022.928944>
PMID:[36061176](https://pubmed.ncbi.nlm.nih.gov/36061176/)
15. Chen CH, Fiecas M, Gutiérrez ED, Panizzon MS, Eyer LT, Vuoksima E, Thompson WK, Fennema-Notestine C, Hagler DJ Jr, Jernigan TL, Neale MC, Franz CE, Lyons MJ, et al. Genetic topography of brain morphology. *Proc Natl Acad Sci USA.* 2013; 110:17089–94.
<https://doi.org/10.1073/pnas.1308091110>
PMID:[24082094](https://pubmed.ncbi.nlm.nih.gov/24082094/)
16. Mueller S, Wang D, Fox MD, Yeo BT, Sepulcre J, Sabuncu MR, Shafee R, Lu J, Liu H. Individual variability in functional connectivity architecture of the human brain. *Neuron.* 2013; 77:586–95.
<https://doi.org/10.1016/j.neuron.2012.12.028>
PMID:[23395382](https://pubmed.ncbi.nlm.nih.gov/23395382/)
17. Buechler R, Wotruba D, Michels L, Theodoridou A, Metzler S, Walitza S, Hänggi J, Kollias S, Rössler W, Heekeren K. Cortical Volume Differences in Subjects at Risk for Psychosis Are Driven by Surface Area. *Schizophr Bull.* 2020; 46:1511–9.
<https://doi.org/10.1093/schbul/sbaa066>
PMID:[32463880](https://pubmed.ncbi.nlm.nih.gov/32463880/)
18. Schmaal L, Yücel M, Ellis R, Vijayakumar N, Simmons JG, Allen NB, Whittle S. Brain Structural Signatures of Adolescent Depressive Symptom Trajectories: A Longitudinal Magnetic Resonance Imaging Study. *J Am Acad Child Adolesc Psychiatry.* 2017; 56:593–601.e9.
<https://doi.org/10.1016/j.jaac.2017.05.008>
PMID:[28647011](https://pubmed.ncbi.nlm.nih.gov/28647011/)
19. Yao N, Winkler AM, Barrett J, Book GA, Beetham T, Horseman R, Leach O, Hodgson K, Knowles EE, Mathias S, Stevens MC, Assaf M, van Erp TG, et al. Inferring pathobiology from structural MRI in schizophrenia and bipolar disorder: Modeling head motion and

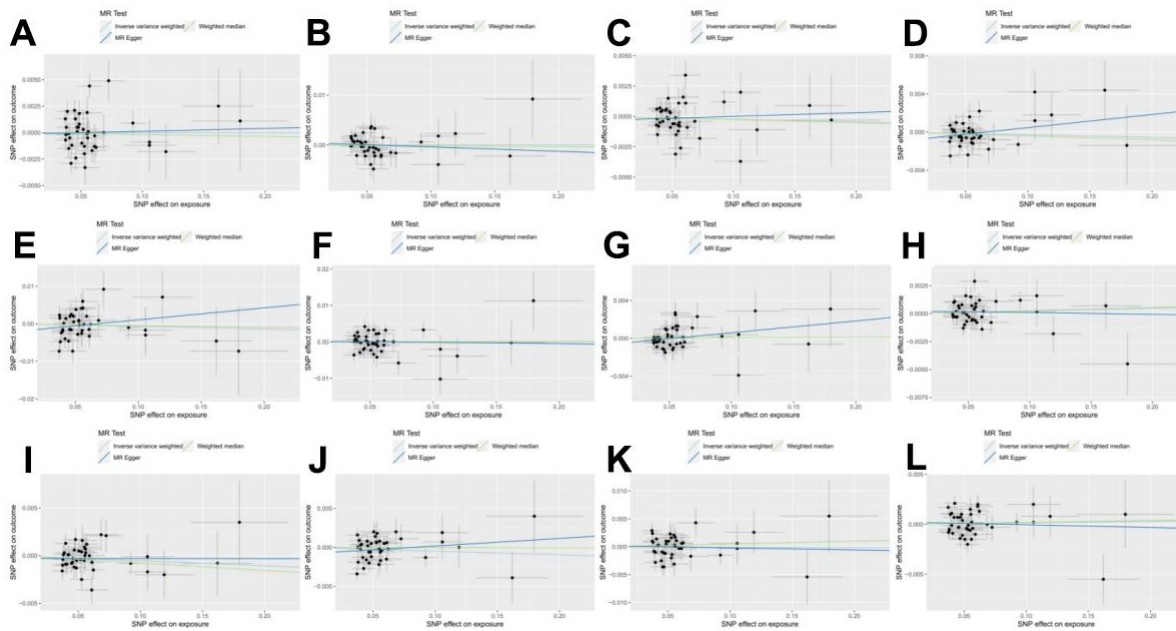
- neuroanatomical specificity. *Hum Brain Mapp.* 2017; 38:3757–70.
<https://doi.org/10.1002/hbm.23612> PMID:28480992
20. Madre M, Canales-Rodríguez EJ, Fuentes-Claramonte P, Alonso-Lana S, Salgado-Pineda P, Guerrero-Pedraza A, Moro N, Bosque C, Gomar JJ, Ortíz-Gil J, Goikolea JM, Bonnin CM, Vieta E, et al. Structural abnormality in schizophrenia versus bipolar disorder: A whole brain cortical thickness, surface area, volume and gyrification analyses. *Neuroimage Clin.* 2020; 25:102131.
<https://doi.org/10.1016/j.nicl.2019.102131>
PMID:31911343
 21. Fleck MS, Daselaar SM, Dobbins IG, Cabeza R. Role of prefrontal and anterior cingulate regions in decision-making processes shared by memory and nonmemory tasks. *Cereb Cortex.* 2006; 16:1623–30.
<https://doi.org/10.1093/cercor/bhj097>
PMID:16400154
 22. Kikinis Z, Fallon JH, Niznikiewicz M, Nestor P, Davidson C, Bobrow L, Pelavin PE, Fischl B, Yendiki A, McCarley RW, Kikinis R, Kubicki M, Shenton ME. Gray matter volume reduction in rostral middle frontal gyrus in patients with chronic schizophrenia. *Schizophr Res.* 2010; 123:153–9.
<https://doi.org/10.1016/j.schres.2010.07.027>
PMID:20822884
 23. Beevers CG, Clasen PC, Enock PM, Schnyer DM. Attention bias modification for major depressive disorder: Effects on attention bias, resting state connectivity, and symptom change. *J Abnorm Psychol.* 2015; 124:463–75.
<https://doi.org/10.1037/abn0000049> PMID:25894440
 24. Japee S, Holiday K, Satyshur MD, Mukai I, Ungerleider LG. A role of right middle frontal gyrus in reorienting of attention: a case study. *Front Syst Neurosci.* 2015; 9:23.
<https://doi.org/10.3389/fnsys.2015.00023>
PMID:25784862
 25. Burgess PW, Gilbert SJ, Dumontheil I. Function and localization within rostral prefrontal cortex (area 10). *Philos Trans R Soc Lond B Biol Sci.* 2007; 362:887–99.
<https://doi.org/10.1098/rstb.2007.2095>
PMID:17403644
 26. Chauhan P, Rathawa A, Jethwa K, Mehra S. The Anatomy of the Cerebral Cortex. In: Pluta R, editor. *Cerebral Ischemia* [Internet]. Brisbane (AU): Exon Publications; 2021.
<https://doi.org/10.36255/exonpublications.cerebralischemia.2021.cerebralcortex> PMID:34905314
 27. Augustine JR. Circuitry and functional aspects of the insular lobe in primates including humans. *Brain Res Brain Res Rev.* 1996; 22:229–44.
[https://doi.org/10.1016/s0165-0173\(96\)00011-2](https://doi.org/10.1016/s0165-0173(96)00011-2)
PMID:8957561
 28. Kurth F, Zilles K, Fox PT, Laird AR, Eickhoff SB. A link between the systems: functional differentiation and integration within the human insula revealed by meta-analysis. *Brain Struct Funct.* 2010; 214:519–34.
<https://doi.org/10.1007/s00429-010-0255-z>
PMID:20512376
 29. Craig AD. How do you feel? Interoception: the sense of the physiological condition of the body. *Nat Rev Neurosci.* 2002; 3:655–66.
<https://doi.org/10.1038/nrn894> PMID:12154366
 30. Craig AD. How do you feel—now? The anterior insula and human awareness. *Nat Rev Neurosci.* 2009; 10:59–70.
<https://doi.org/10.1038/nrn2555> PMID:19096369
 31. Knutson KM, Rakowsky ST, Solomon J, Krueger F, Raymont V, Tierney MC, Wassermann EM, Grafman J. Injured brain regions associated with anxiety in Vietnam veterans. *Neuropsychologia.* 2013; 51:686–94.
<https://doi.org/10.1016/j.neuropsychologia.2013.01.003> PMID:23328629
 32. Knutson KM, Dal Monte O, Raymont V, Wassermann EM, Krueger F, Grafman J. Neural correlates of apathy revealed by lesion mapping in participants with traumatic brain injuries. *Hum Brain Mapp.* 2014; 35:943–53.
<https://doi.org/10.1002/hbm.22225>
PMID:23404730
 33. Geng J, Yan R, Shi J, Chen Y, Mo Z, Shao J, Wang X, Yao Z, Lu Q. Altered regional homogeneity in patients with somatic depression: A resting-state fMRI study. *J Affect Disord.* 2019; 246:498–505.
<https://doi.org/10.1016/j.jad.2018.12.066>
PMID:30599374
 34. Cheng W, Rolls ET, Qiu J, Liu W, Tang Y, Huang CC, Wang X, Zhang J, Lin W, Zheng L, Pu J, Tsai SJ, Yang AC, et al. Medial reward and lateral non-reward orbitofrontal cortex circuits change in opposite directions in depression. *Brain.* 2016; 139:3296–309.
<https://doi.org/10.1093/brain/aww255>
PMID:27742666
 35. de Coster L, Leentjens AF, Lodder J, Verhey FR. The sensitivity of somatic symptoms in post-stroke depression: a discriminant analytic approach. *Int J Geriatr Psychiatry.* 2005; 20:358–62.
<https://doi.org/10.1002/gps.1290> PMID:15799083
 36. Kompus K, Hugdahl K, Ohman A, Marklund P, Nyberg L. Distinct control networks for cognition and emotion in the prefrontal cortex. *Neurosci Lett.* 2009; 467:76–80.

- <https://doi.org/10.1016/j.neulet.2009.10.005>
PMID:19818382
37. Qiu L, Su J, Ni Y, Bai Y, Zhang X, Li X, Wan X. The neural system of metacognition accompanying decision-making in the prefrontal cortex. *PLoS Biol.* 2018; 16:e2004037.
<https://doi.org/10.1371/journal.pbio.2004037>
PMID:29684004
38. Młyniec K, Doboszewska U, Szewczyk B, Sowa-Kućma M, Misztak P, Piekoszewski W, Trela F, Ostachowicz B, Nowak G. The involvement of the GPR39-Zn(2+)-sensing receptor in the pathophysiology of depression. *Studies in rodent models and suicide victims. Neuropharmacology.* 2014; 79:290–7.
<https://doi.org/10.1016/j.neuropharm.2013.12.001>
PMID:24333148
39. Holst B, Egerod KL, Schild E, Vickers SP, Cheetham S, Gerlach LO, Storjohann L, Stidsen CE, Jones R, Beck-Sickinger AG, Schwartz TW. GPR39 signaling is stimulated by zinc ions but not by obestatin. *Endocrinology.* 2007; 148:13–20.
<https://doi.org/10.1210/en.2006-0933>
PMID:16959833
40. Młyniec K, Budziszewska B, Reczyński W, Sowa-Kućma M, Nowak G. The role of the GPR39 receptor in zinc deficient-animal model of depression. *Behav Brain Res.* 2013; 238:30–5.
<https://doi.org/10.1016/j.bbr.2012.10.020>
PMID:23089648
41. Holst B, Holliday ND, Bach A, Elling CE, Cox HM, Schwartz TW. Common structural basis for constitutive activity of the ghrelin receptor family. *J Biol Chem.* 2004; 279:53806–17.
<https://doi.org/10.1074/jbc.M407676200>
PMID:15383539
42. Petrilli MA, Kranz TM, Kleinhaus K, Joe P, Getz M, Johnson P, Chao MV, Malaspina D. The Emerging Role for Zinc in Depression and Psychosis. *Front Pharmacol.* 2017; 8:414.
<https://doi.org/10.3389/fphar.2017.00414>
PMID:28713269
43. Młyniec K, Nowak G. Up-regulation of the GPR39 Zn2+-sensing receptor and CREB/BDNF/TrkB pathway after chronic but not acute antidepressant treatment in the frontal cortex of zinc-deficient mice. *Pharmacol Rep.* 2015; 67:1135–40.
<https://doi.org/10.1016/j.pharep.2015.04.003>
PMID:26481532
44. Gilad D, Shorer S, Ketzef M, Friedman A, Sekler I, Aizenman E, Hershinkel M. Homeostatic regulation of KCC2 activity by the zinc receptor mZnR/GPR39 during seizures. *Neurobiol Dis.* 2015; 81:4–13.
<https://doi.org/10.1016/j.nbd.2014.12.020>
PMID:25562657
45. Besser L, Chorin E, Sekler I, Silverman WF, Atkin S, Russell JT, Hershinkel M. Synaptically released zinc triggers metabotropic signaling via a zinc-sensing receptor in the hippocampus. *J Neurosci.* 2009; 29:2890–901.
<https://doi.org/10.1523/JNEUROSCI.5093-08.2009>
PMID:19261885
46. Saadi RA, He K, Hartnett KA, Kandler K, Hershinkel M, Aizenman E. SNARE-dependent upregulation of potassium chloride co-transporter 2 activity after metabotropic zinc receptor activation in rat cortical neurons *in vitro*. *Neuroscience.* 2012; 210:38–46.
<https://doi.org/10.1016/j.neuroscience.2012.03.001>
PMID:22441041
47. Rychlik M, Młyniec K. Zinc-mediated Neurotransmission in Alzheimer’s Disease: A Potential Role of the GPR39 in Dementia. *Curr Neuropharmacol.* 2020; 18:2–13.
<https://doi.org/10.2174/1570159X17666190704153807>
PMID:31272355
48. Młyniec K, Gawęł M, Librowski T, Reczyński W, Bystrowska B, Holst B. Investigation of the GPR39 zinc receptor following inhibition of monoaminergic neurotransmission and potentialization of glutamatergic neurotransmission. *Brain Res Bull.* 2015; 115:23–9.
<https://doi.org/10.1016/j.brainresbull.2015.04.005>
PMID:25917396
49. Yang C, Hu G, Li Z, Wang Q, Wang X, Yuan C, Wang Z, Hong W, Lu W, Cao L, Chen J, Wang Y, Yu S, et al. Differential gene expression in patients with subsyndromal symptomatic depression and major depressive disorder. *PLoS One.* 2017; 12:e0172692.
<https://doi.org/10.1371/journal.pone.0172692>
PMID:28333931
50. Li D, Musante V, Zhou W, Picciotto MR, Nairn AC. Striatin-1 is a B subunit of protein phosphatase PP2A that regulates dendritic arborization and spine development in striatal neurons. *J Biol Chem.* 2018; 293:11179–94.
<https://doi.org/10.1074/jbc.RA117.001519>
PMID:29802198
51. Andersen H, Braestrup C, Randrup A. Apomorphine-induced stereotyped biting in the tortoise in relation to dopaminergic mechanisms. *Brain Behav Evol.* 1975; 11:365–73.
<https://doi.org/10.1159/000123646>
PMID:1238150
52. Lin L, Hales CM, Garber K, Jin P. Fat mass and obesity-associated (FTO) protein interacts with CaMKII and

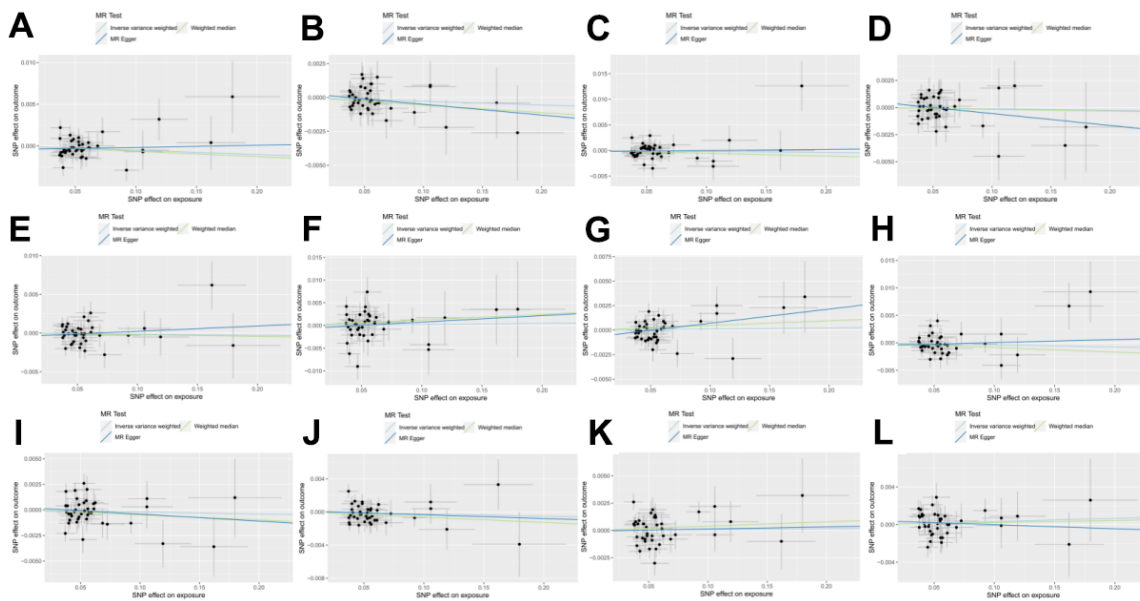
- modulates the activity of CREB signaling pathway. *Hum Mol Genet.* 2014; 23:3299–306.
<https://doi.org/10.1093/hmg/ddu043>
PMID:[24488767](https://pubmed.ncbi.nlm.nih.gov/24488767/)
53. Yan X, Liu J, Ye Z, Huang J, He F, Xiao W, Hu X, Luo Z. CaMKII-Mediated CREB Phosphorylation Is Involved in Ca²⁺-Induced BDNF mRNA Transcription and Neurite Outgrowth Promoted by Electrical Stimulation. *PLoS One.* 2016; 11:e0162784.
<https://doi.org/10.1371/journal.pone.0162784>
PMID:[27611779](https://pubmed.ncbi.nlm.nih.gov/27611779/)
54. Song SH, Augustine GJ. Synapsin Isoforms and Synaptic Vesicle Trafficking. *Mol Cells.* 2015; 38:936–40.
<https://doi.org/10.14348/molcells.2015.0233>
PMID:[26627875](https://pubmed.ncbi.nlm.nih.gov/26627875/)
55. Shen J, Yang L, Wei W. Role of Fto on CaMKII/CREB signaling pathway of hippocampus in depressive-like behaviors induced by chronic restraint stress mice. *Behav Brain Res.* 2021; 406:113227.
<https://doi.org/10.1016/j.bbr.2021.113227>
PMID:[33677012](https://pubmed.ncbi.nlm.nih.gov/33677012/)
56. Rozanski A. Behavioral cardiology: current advances and future directions. *J Am Coll Cardiol.* 2014; 64:100–10.
<https://doi.org/10.1016/j.jacc.2014.03.047>
PMID:[24998134](https://pubmed.ncbi.nlm.nih.gov/24998134/)
57. Lichtman JH, Froelicher ES, Blumenthal JA, Carney RM, Doering LV, Frasure-Smith N, Freedland KE, Jaffe AS, Leifheit-Limson EC, Sheps DS, Vaccarino V, Wulsin L, and American Heart Association Statistics Committee of the Council on Epidemiology and Prevention and the Council on Cardiovascular and Stroke Nursing. Depression as a risk factor for poor prognosis among patients with acute coronary syndrome: systematic review and recommendations: a scientific statement from the American Heart Association. *Circulation.* 2014; 129:1350–69.
<https://doi.org/10.1161/CIR.000000000000019>
PMID:[24566200](https://pubmed.ncbi.nlm.nih.gov/24566200/)
58. Jefferson JW. Psychocardiology: meeting place of heart and mind. *Psychosomatics.* 1985; 26:841–2.
[https://doi.org/10.1016/S0033-3182\(85\)72774-0](https://doi.org/10.1016/S0033-3182(85)72774-0)
PMID:[4080931](https://pubmed.ncbi.nlm.nih.gov/4080931/)

SUPPLEMENTARY MATERIALS

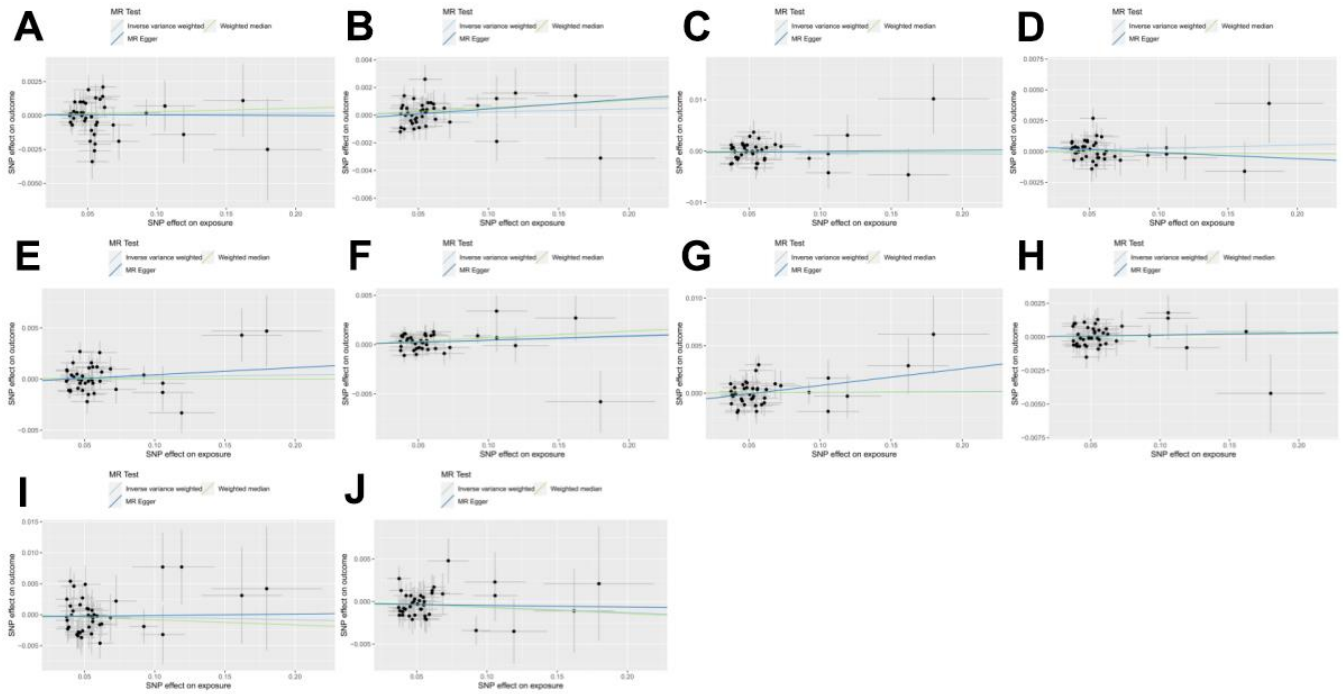
Supplementary Figures



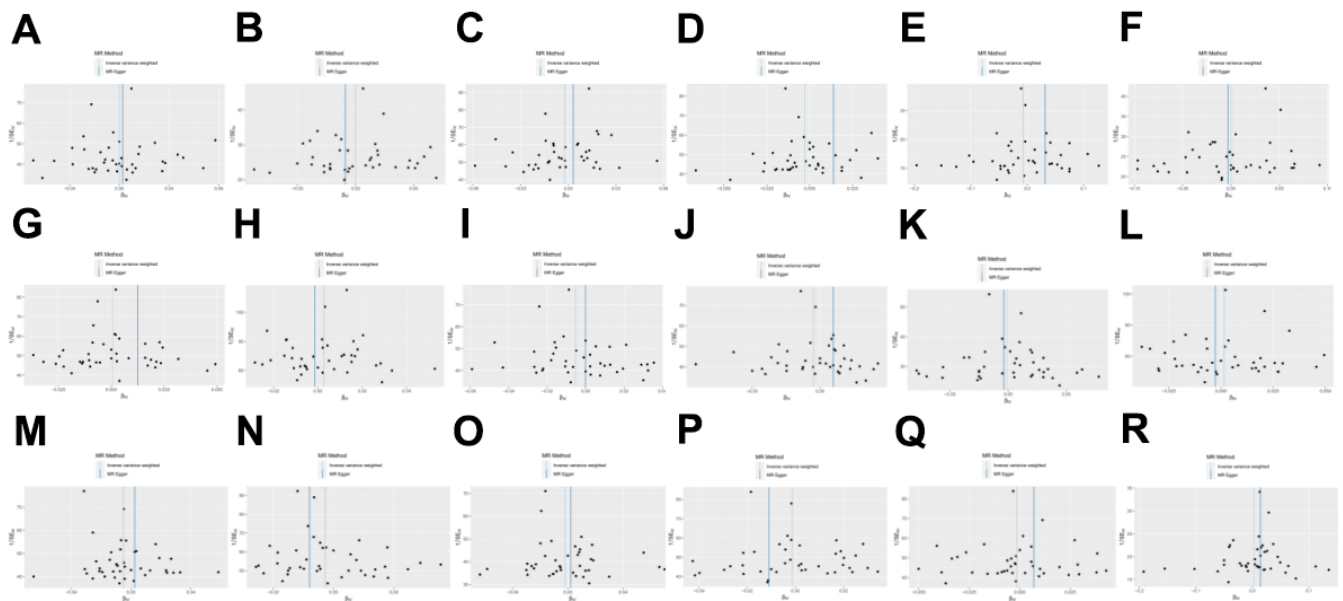
Supplementary Figure 1. MR scatter plots of the relationship between heart failure and cortical thickness in cerebral functional areas 1. (A) Banksst, (B) caudal anterior cingulate, (C) caudal middle frontal, (D) cuneus, (E) entorhinal, (F) frontal pole, (G) fusiform, (H) inferior parietal, (I) inferior temporal, (J) insula, (K) isthmus cingulate, (L) lateral occipital.



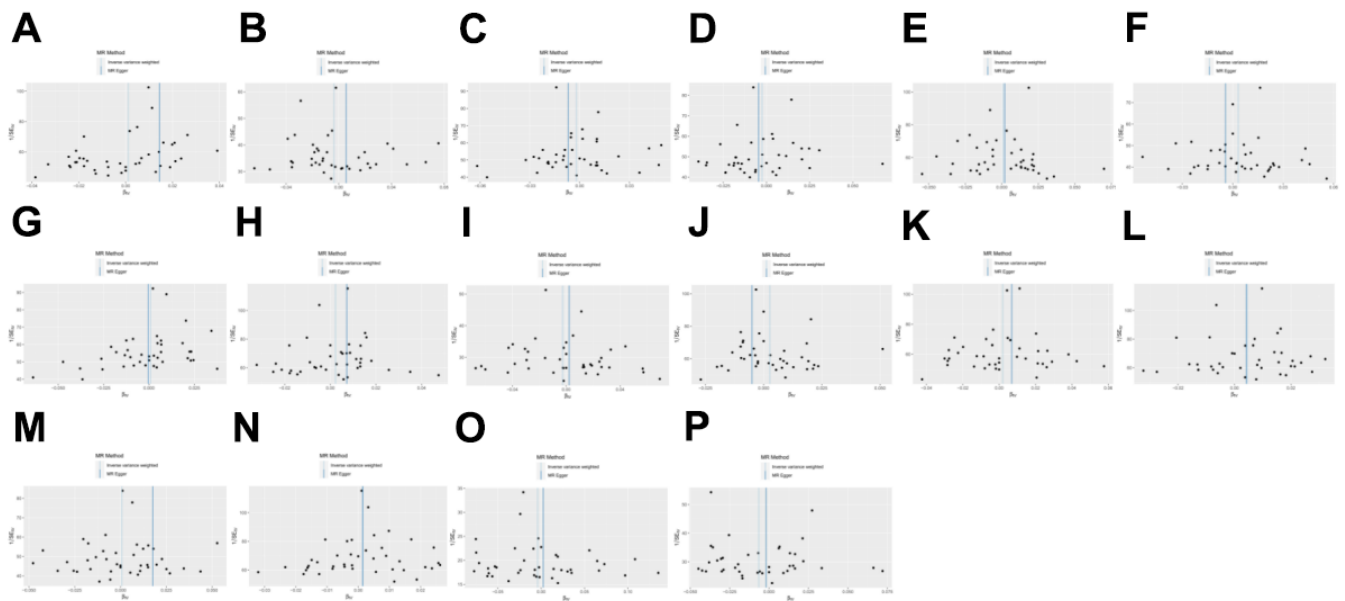
Supplementary Figure 2. MR scatter plots of the relationship between heart failure and cortical thickness in cerebral functional areas 2. (A) Lateral orbitofrontal, (B) lingual, (C) posterior cingulate medial orbitofrontal, (D) middle temporal, (E) paracentral, (F) parahippocampal, (G) pars opercularis, (H) pars orbitalis, (I) pars triangularis, (J) pericalcarine, (K) postcentral, (L) posterior cingulate.



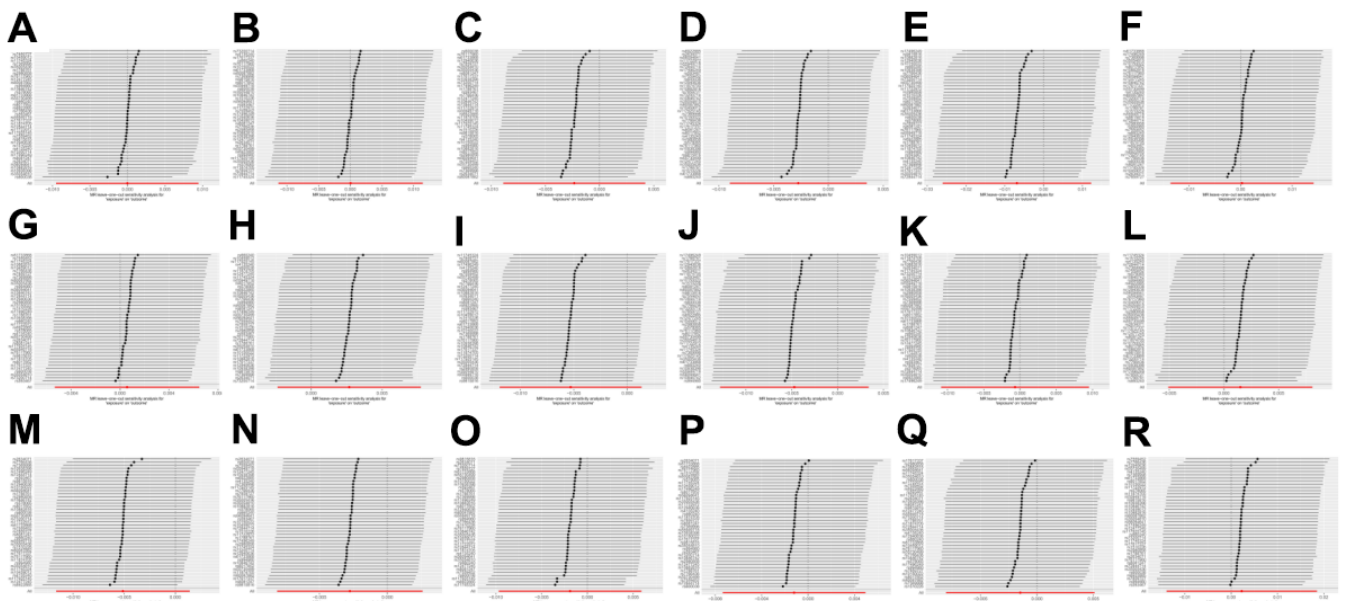
Supplementary Figure 3. MR scatter plots of the relationship between heart failure and cortical thickness in cerebral functional areas 3. (A) Precentral, (B) precuneus, (C) rostral anterior cingulate, (D) rostral middle frontal, (E) superior frontal, (F) superior parietal, (G) superior temporal, (H) supramarginal, (I) temporal pole, (J) transverse temporal.



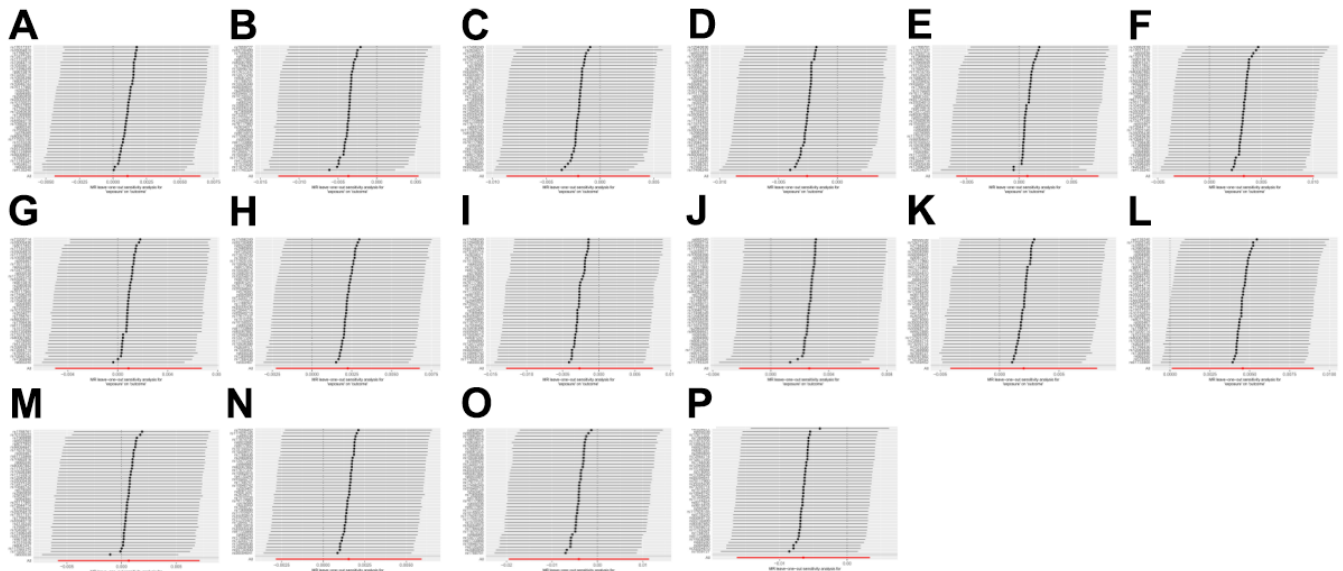
Supplementary Figure 4. Funnel plot 1 of heterogeneity test results of the relationship between heart failure and cerebral functional area cortex thickness by MR. (A) Bankssts, (B) caudal anterior cingulate, (C) caudal middle frontal, (D) cuneus, (E) entorhinal, (F) frontal pole, (G) fusiform, (H) inferior parietal, (I) inferior temporal, (J) insula, (K) isthmus cingulate, (L) lateral occipital, (M) lateral orbitofrontal, (N) lingual, (O) medial orbitofrontal, (P) middle temporal, (Q) paracentral, (R) parahippocampal.



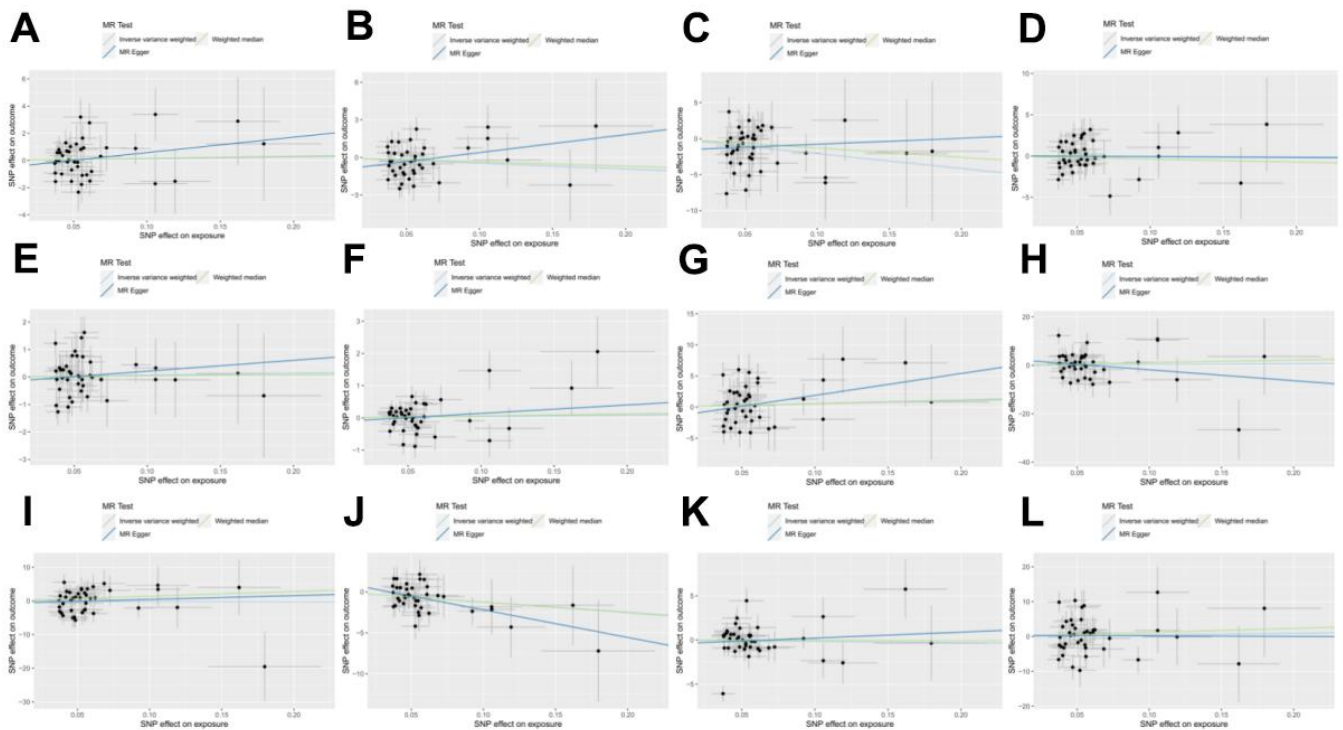
Supplementary Figure 5. Funnel plot 2 of heterogeneity test results of the relationship between heart failure and cerebral functional area cortex thickness by MR. (A) Pars opercularis, (B) pars orbitalis, (C) pars triangularis, (D) pericalcarine, (E) postcentral, (F) posterior cingulate, (G) precentral, (H) precuneus, (I) rostral anterior cingulate, (J) rostral middle frontal, (K) superior frontal, (L) superior parietal, (M) superior temporal, (N) supramarginal, (O) temporal pole, (P) transverse temporal.



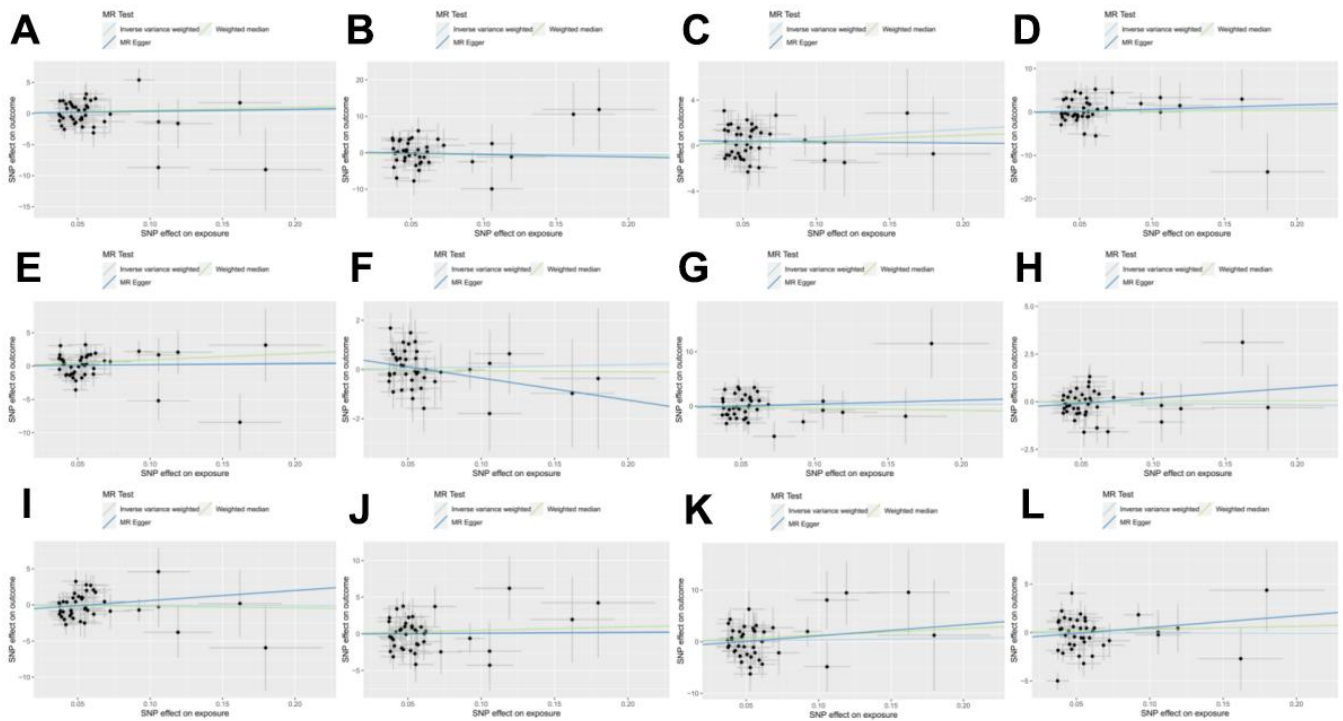
Supplementary Figure 6. "Leave-one-out" forest map 1 of MR analysis of in the relationship between heart failure and the cortical thickness of brain functional areas. (A) Bankssts, (B) caudal anterior cingulate, (C) caudal middle frontal, (D) cuneus, (E) entorhinal, (F) frontal pole, (G) fusiform, (H) inferior parietal, (I) inferior temporal, (J) insula, (K) isthmus cingulate, (L) lateral occipital, (M) lateral orbitofrontal, (N) lingual, (O) medial orbitofrontal, (P) middle temporal, (Q) paracentral, (R) parahippocampal.



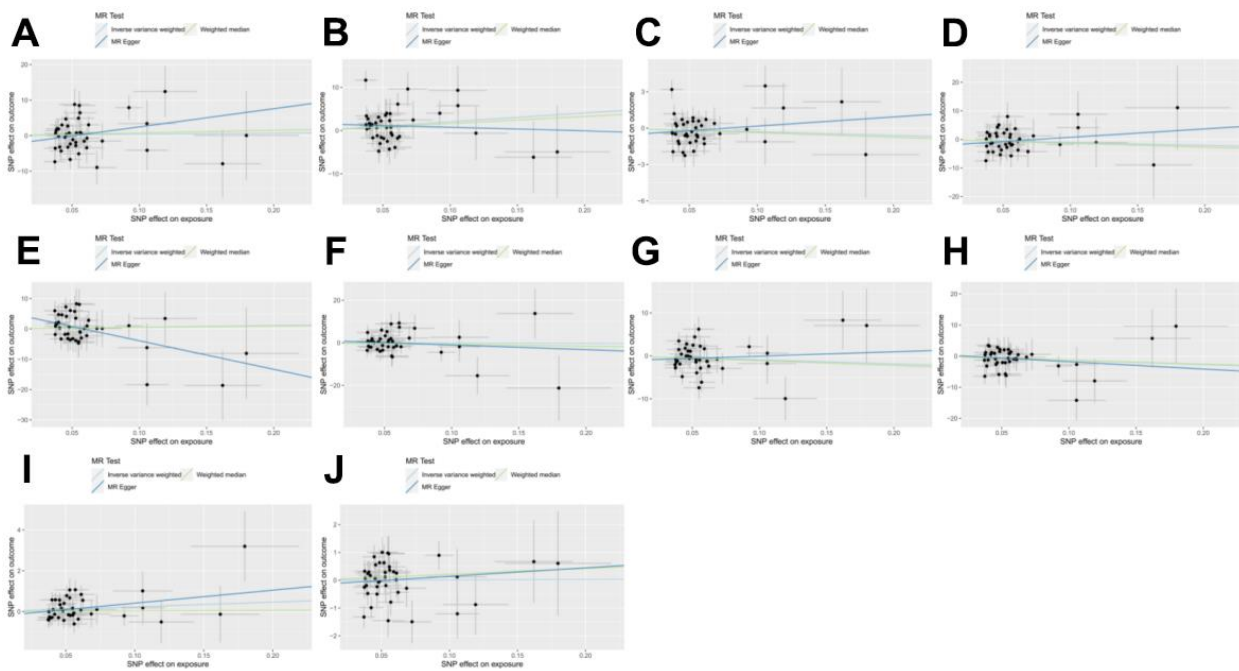
Supplementary Figure 7. "Leave-one-out" forest map 2 of MR analysis of in the relationship between heart failure and the cortical thickness of functional brain areas. (A) Pars opercularis, (B) pars orbitalis, (C) pars triangularis, (D) pericalcarine, (E) postcentral, (F) posterior cingulate, (G) precentral, (H) precuneus, (I) rostral anterior cingulate, (J) rostral middle frontal, (K) superior frontal, (L) superior parietal, (M) superior temporal, (N) supramarginal, (O) temporal pole, (P) transverse temporal.



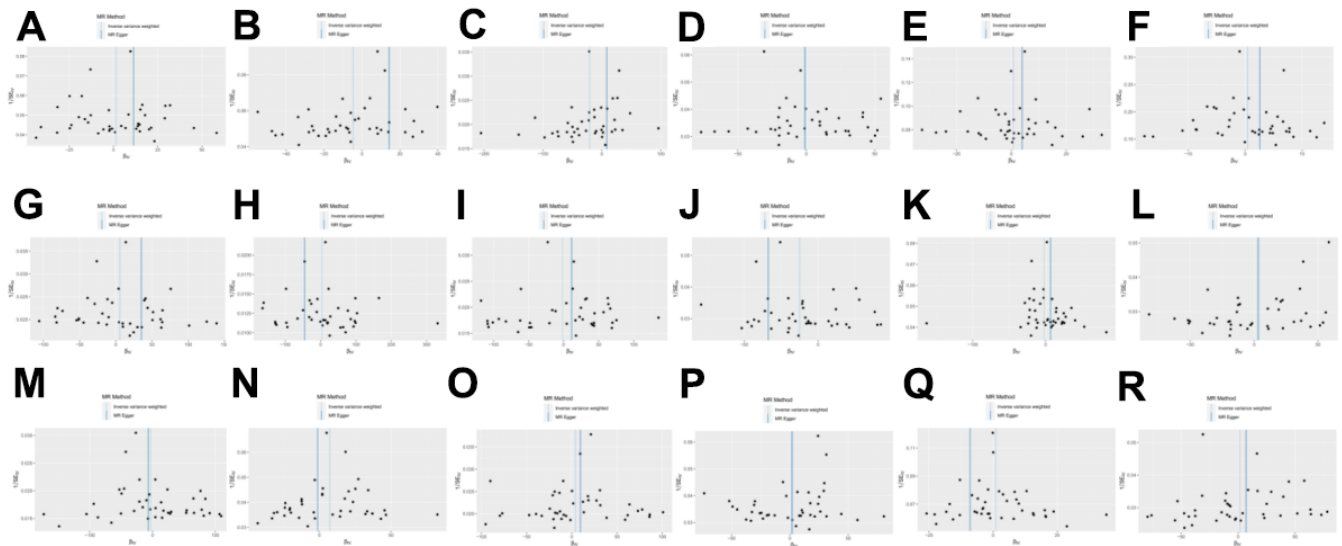
Supplementary Figure 8. MR scatter plot 1 of the relationship between heart failure and the cortical surface area of functional brain areas. (A) Banksst, (B) caudal anterior cingulate, (C) caudal middle frontal, (D) cuneus, (E) entorhinal, (F) frontal pole, (G) fusiform, (H) inferior parietal, (I) inferior temporal, (J) insula, (K) isthmus cingulate, (L) lateral occipital.



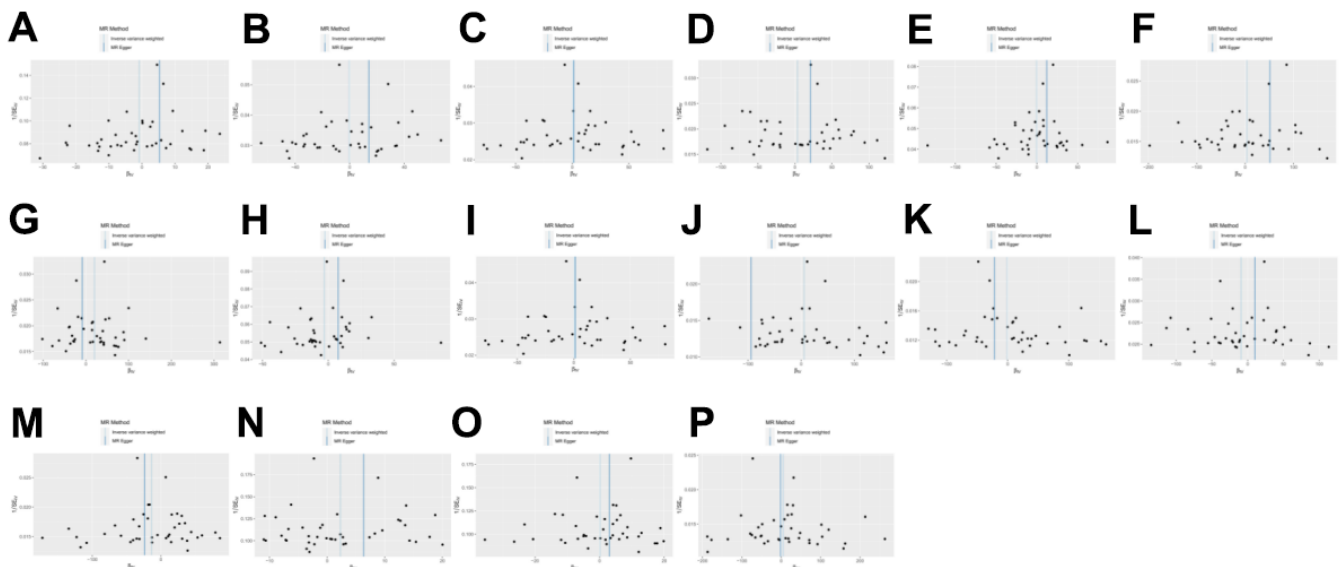
Supplementary Figure 9. MR scatter plot 2 of the relationship between heart failure and the cortical surface area of functional brain areas. (A) Lateral orbitofrontal, (B) lingual, (C) posterior cingulate medial orbitofrontal, (D) middle temporal, (E) paracentral, (F) parahippocampal, (G) pars opercularis, (H) pars orbitalis, (I) pars triangularis, (J) pericalcarine, (K) postcentral, (L) posterior cingulate.



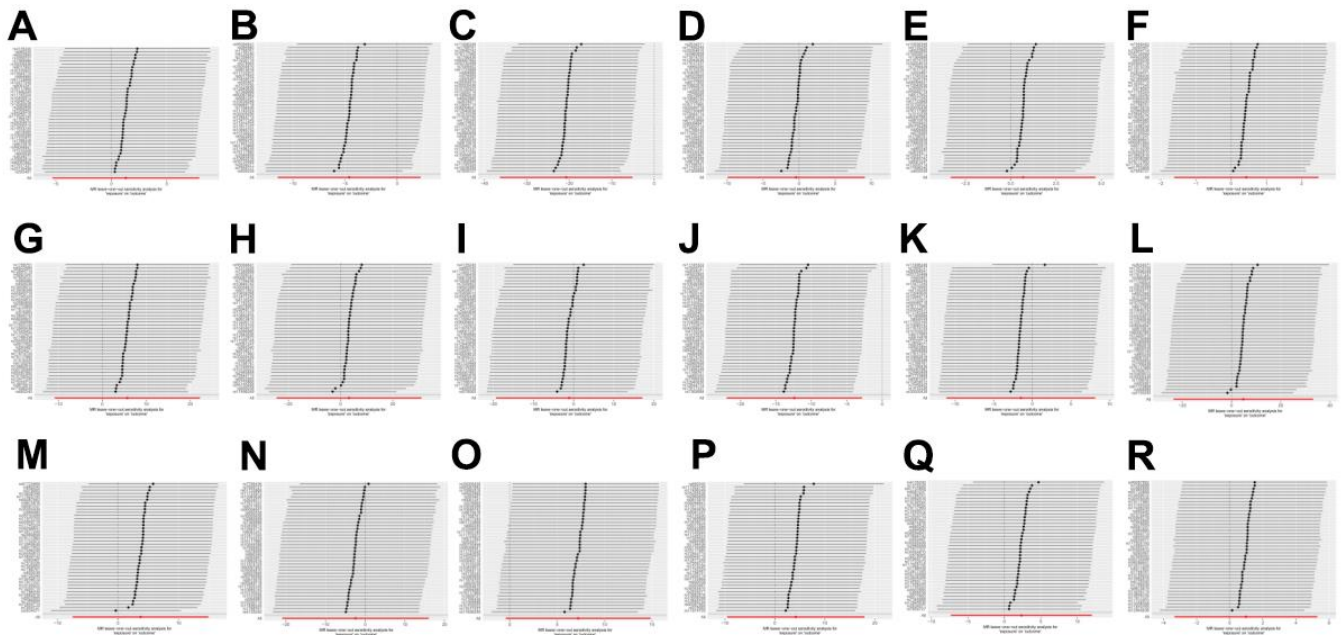
Supplementary Figure 10. MR scatter plot 3 of the relationship between heart failure and the cortical surface area of functional brain areas. (A) Precentral, (B) precuneus, (C) rostral anterior cingulate, (D) rostral middle frontal, (E) superior frontal, (F) superior parietal, (G) superior temporal, (H) supramarginal, (I) temporal pole, (J) transverse temporal.



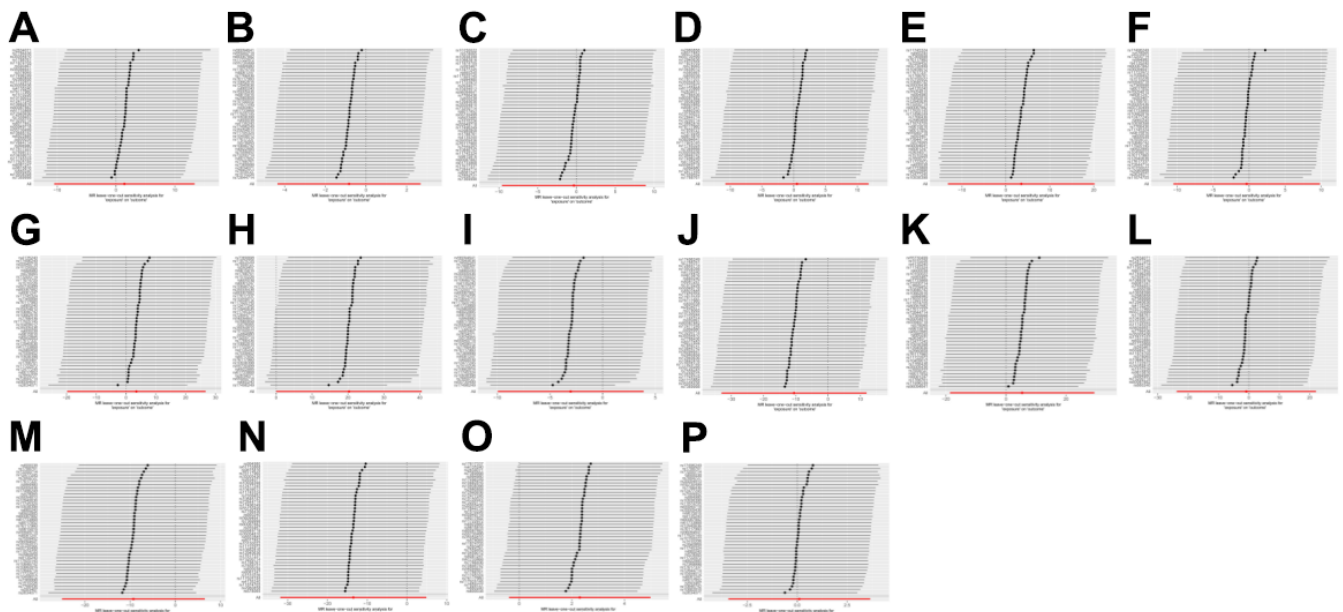
Supplementary Figure 11. Funnel plot 1 of heterogeneity test results of MR analysis of the relationship between heart failure and the cortical surface area of functional cerebral areas. (A) Bankssts, (B) caudal anterior cingulate, (C) caudal middle frontal, (D) cuneus, (E) entorhinal, (F) frontal pole, (G) fusiform, (H) inferior parietal, (I) inferior temporal, (J) insula, (K) isthmus cingulate, (L) lateral occipital, (M) lateral orbitofrontal, (N) lingual, (O) medial orbitofrontal, (P) middle temporal, (Q) paracentral, (R) parahippocampal.



Supplementary Figure 12. Funnel plot 2 of heterogeneity test results of MR analysis of in the relationship between heart failure and the cortical surface area of functional cerebral areas. (A) Pars opercularis, (B) pars orbitalis, (C) pars triangularis, (D) pericalcarine, (E) postcentral, (F) posterior cingulate, (G) precentral, (H) precuneus, (I) rostral anterior cingulate, (J) rostral middle frontal, (K) superior frontal, (L) superior parietal, (M) superior temporal, (N) supramarginal, (O) temporal pole, (P) transverse temporal.



Supplementary Figure 13. "Leave-one-out" forest map 1 of MR analysis of the relationship between heart failure and the cortical surface area of functional brain areas. (A) Bankssts, (B) caudal anterior cingulate, (C) caudal middle frontal, (D) cuneus, (E) entorhinal, (F) frontal pole, (G) fusiform, (H) inferior parietal, (I) inferior temporal, (J) insula, (K) isthmus cingulate, (L) lateral occipital, (M) lateral orbitofrontal, (N) lingual, (O) medial orbitofrontal, (P) middle temporal, (Q) paracentral, (R) parahippocampal.



Supplementary Figure 14. "Leave-one-out" forest map 2 of MR analysis of the relationship between heart failure and the cortical surface area of functional brain areas. (A) Pars opercularis, (B) pars orbitalis, (C) pars triangularis, (D) pericalcarine, (E) postcentral, (F) posterior cingulate, (G) precentral, (H) precuneus, (I) rostral anterior cingulate, (J) rostral middle frontal, (K) superior frontal, (L) superior parietal, (M) superior temporal, (N) supramarginal, (O) temporal pole, (P) transverse temporal.

Supplementary Tables

Supplementary Table 1. Basic information of SNPs associated with heart failure.

SNPs	other_allele	effect_allele	β	SE	P
rs55751848	C	G	-0.0425	0.0089	1.79E-06
rs593467	G	A	-0.0548	0.0118	3.42E-06
rs660240	T	C	0.0611	0.0097	3.00E-10
rs35054810	G	A	0.0725	0.0143	3.98E-07
rs7559452	A	G	0.0468	0.0102	4.47E-06
rs17496249	A	G	-0.0372	0.0079	2.49E-06
rs12477245	C	T	0.1192	0.0236	4.40E-07
rs7369998	G	A	-0.059	0.0126	2.83E-06
rs72844714	C	A	0.0559	0.0121	3.84E-06
rs80087882	G	A	0.0609	0.0125	1.10E-06
rs4376020	T	A	-0.0612	0.0123	6.50E-07
rs9815816	T	C	0.0479	0.0099	1.31E-06
rs10938398	G	A	0.0389	0.008	1.16E-06
rs11722972	T	G	-0.0519	0.0114	5.30E-06
rs2634071	T	C	-0.0923	0.0101	6.33E-20
rs11745324	G	A	-0.0528	0.0095	2.73E-08
rs7766436	C	T	0.04	0.0086	3.30E-06
rs4135240	T	C	-0.0486	0.0084	7.22E-09
rs6922885	T	C	-0.0377	0.008	2.45E-06
rs55949718	C	T	-0.0685	0.0142	1.41E-06
rs1510226	T	C	0.162	0.0285	1.31E-08
rs55730499	C	T	0.1058	0.0157	1.60E-11
rs117925145	A	G	0.1797	0.0391	4.31E-06
rs76117960	T	C	0.0528	0.0113	2.97E-06
rs35005436	T	C	0.0533	0.0116	4.33E-06
rs10952517	T	A	-0.0394	0.0085	3.56E-06
rs73200714	G	A	-0.055	0.0118	3.15E-06
rs2980858	T	C	-0.04	0.0086	3.30E-06
rs7859727	C	T	0.0623	0.0078	1.38E-15
rs600038	T	C	0.0569	0.0096	3.08E-09
rs994980	C	T	0.0375	0.0081	3.66E-06
rs72807031	T	A	-0.0895	0.0181	7.62E-07
rs4746140	G	C	-0.0666	0.0109	9.96E-10
rs10882816	G	T	-0.0447	0.0085	1.45E-07
rs17617337	C	T	-0.0561	0.0095	3.52E-09
rs61733868	T	C	-0.1057	0.0216	9.90E-07
rs186973337	T	A	0.0933	0.0196	1.93E-06
rs4755717	C	G	-0.0379	0.008	2.16E-06
rs10459012	C	A	0.0458	0.0095	1.43E-06
rs12805761	A	T	-0.0672	0.0139	1.33E-06
rs4766578	T	A	-0.0433	0.0079	4.23E-08
rs10846742	G	A	-0.0506	0.0111	5.15E-06
rs8017852	C	A	-0.0554	0.012	3.90E-06
rs10150022	A	G	-0.0419	0.0087	1.46E-06

rs17483686	A	T	0.0489	0.0095	2.64E-07
rs56094641	A	G	0.0454	0.008	1.39E-08
rs578065	T	G	0.0408	0.0082	6.50E-07
rs12940636	T	C	-0.0381	0.0083	4.42E-06
rs8081247	G	A	-0.0487	0.0098	6.72E-07
rs1788761	A	G	-0.0425	0.009	2.33E-06
rs11874705	A	G	0.0469	0.0098	1.70E-06
rs10520390	C	G	-0.0902	0.0187	1.41E-06

Supplementary Table 2. MR results of the effect of heart failure on the cortical structure of functional cerebral areas.

	SA	TH
	Global weighted	
Bankssts	0.6977748	0.9969515
Caudal anterior cingulate	0.1879553	0.9944418
Caudal middle frontal	0.009369889	0.4861102
Cuneus	0.93282	0.3884087
Entorhinal	0.7375308	0.4824811
Frontal pole	0.6806647	0.9700872
Fusiform	0.5006216	0.8486323
Inferior parietal	0.8200912	0.2974922
Inferior temporal	0.9055626	0.1172891
Insula	0.01088126	0.2536509
Isthmus cingulate	0.7616352	0.8956049
Lateral occipital	0.740052	0.6561721
Lateral orbitofrontal	0.5156932	0.1242299
Lingual	0.7964685	0.3125903
Medial orbitofrontal	0.06407264	0.6340118
Middle temporal	0.5498127	0.6994723
Paracentral	0.6369187	0.6598778
Parahippocampal	0.6559629	0.7828665
Pars opercularis	0.8144172	0.6971543
Par orbitalis	0.6418063	0.4258328
Pars triangularis	0.9436559	0.5506617
Pericalcarine	0.9299025	0.4058616
Postcentral	0.6802846	0.8207215
Posterior cingulate	0.9478465	0.3376118
Precentral	0.7710834	0.773043
Precuneus	0.0496107	0.3306158
Rostral anterior cingulate	0.3899105	0.6066478
Rostral middle frontal	0.3578567	0.2814057
Superior frontal	0.66020664	0.5205543
Superior parietal	0.9424974	0.04477682
Superior temporal	0.2498117	0.843193
Supramarginal	0.1505051	0.4930569
Temporal pole	0.09355074	0.6033848
Transverse temporal	0.9531146	0.1976769

Supplementary Table 3. MR pleiotropic analysis of cortical thickness in cerebral functional areas in heart failure patients.

Cerebral cortex	Egger-intercept	SE	P
Bankssts	-0.000151779	0.000882834	0.8643876
Caudal anterior cingulate	0.000487773	0.00104738	0.6440152
Caudal middle frontal	-0.000299749	0.000605053	0.623091
Cuneus	-0.000922428	0.000574205	0.1162442
Entorhinal	-0.002141749	0.001745485	0.22717
Frontal pole	0.000195246	0.001289201	0.8804034
Fusiform	-0.000658134	0.000539236	0.2296064
Inferior parietal	0.000226421	0.0004656	0.6294766
Inferior temporal	-0.0002893	0.000607283	0.6364592
Insula	-0.000799705	0.000735893	0.2838346
Isthmus cingulate	0.000161048	0.000943923	0.865408
Lateral occipital	0.000234886	0.000612812	0.7035848
Lateral orbitofrontal	-0.000424334	0.000596338	0.4809688
Lingual	0.000286671	0.000493235	0.5644465
Medial orbitofrontal	-0.000220342	0.000722794	0.7621033
Middle temporal	0.000546603	0.000566318	0.3403976
Paracentral	-0.000464085	0.000608095	0.4499489
Parahippocampal	-0.000661862	0.001500857	0.6616559
Pars opercularis	-0.00073961	0.000494173	0.1425313
Pars orbitalis	-0.000512167	0.0008384	0.5448189
Pars triangularis	0.000264559	0.000619918	0.671898
Pericalcarine	0.000108325	0.000558845	0.847309
Postcentral	-6.45318E-05	0.000631108	0.9190809
Posterior cingulate	0.000420647	0.000618175	0.5002296
Precentral	6.53192E-05	0.000544684	0.9051611
Precuneus	-0.000272092	0.000417158	0.5180639
Rostral anterior cingulate	-0.000270701	0.000929568	0.7724327
Rostral middle frontal	0.000424245	0.000443086	0.3442245
Superior frontal	-0.000272435	0.000581861	0.6422378
Superior parietal	2.09165E-05	0.000411503	0.9597207
Superior temporal	-0.000939761	0.000581243	0.1139801
Supramarginal	6.47205E-06	0.00040376	0.9872926
Temporal pole	-0.000355457	0.001417925	0.803371
Transverse temporal	-0.000251782	0.000907365	0.7828721

Supplementary Table 4. MR pleiotropic analysis of cortical surface area of cerebral functional area in heart failure.

Cerebral cortex	Egger-intercept	SE	P
Bankssts	-0.5550066	0.6080988	0.3670126
Caudal anterior cingulate	-1.047564	0.6136488	0.09575322
Caudal middle frontal	-1.608463	1.42652	0.2664022
Cuneus	0.03487043	0.8842244	0.9687438
Entorhinal	-0.1806707	0.3692631	0.6273886
Frontal pole	-0.1204245	0.189236	0.5282514
Fusiform	-1.631361	1.515063	0.2882028
Inferior parietal	2.67364	2.543369	0.2996279
Inferior temporal	-0.6900998	1.686612	0.684658
Insula	1.182193	0.8740075	0.1839702
Isthmus cingulate	-0.4546133	0.8927734	0.613471
Lateral occipital	0.3568113	2.634551	0.8929643
Lateral orbitofrontal	0.03948283	1.03887	0.9698771
Lingual	0.2514821	1.712191	0.8839855
Medial orbitofrontal	0.4619694	0.703708	0.5153712
Middle temporal	-0.2951111	1.265819	0.8168732
Paracentral	0.04591706	0.8976835	0.9594666
Parahippocampal	0.5518967	0.394956	0.1702041
Pars opercularis	-0.3101397	1.105776	0.7805976
Pars orbitalis	-0.3421035	0.321653	0.2940605
Pars triangularis	-0.7926667	0.8503531	0.356988
Pericalcarine	-0.04470478	1.03377	0.9657274
Postcentral	-0.9813764	1.542445	0.5283318
Posterior cingulate	-0.68538	0.9402103	0.4703785
Precentral	-2.642603	2.116006	0.2191595
Precuneus	1.577018	1.865732	0.4031248
Rostral anterior cingulate	-0.5860225	0.6358936	0.3624173
Rostral middle frontal	-2.219558	2.060125	0.2879254
Superior frontal	5.515524	2.069316	0.01112991
Superior parietal	1.161043	2.1021	0.5838773
Superior temporal	-1.075803	1.45459	0.4639763
Supramarginal	0.5605873	1.683823	0.7409738
Temporal pole	-0.2244677	0.2469013	0.3688609
Transverse temporal	-0.1623271	0.3284371	0.6239085

Supplementary Table 5. MR sensitivity analysis of cortical thickness in cerebral functional areas in heart failure patients.

Cerebral cortex	Method	Cochran's Q	P
Bankssts	MR-Egger	75.7908	0.00037696
	Inverse variance weighted	75.84828	0.000533208
Caudal anterior cingulate	MR-Egger	33.69524	0.7101431
	Inverse variance weighted	33.91213	0.7398873
Caudal middle frontal	MR-Egger	56.01457	0.03798923
	Inverse variance weighted	56.36708	0.04463329
Cuneus	MR-Egger	35.3256	0.6382164
	Inverse variance weighted	37.90626	0.5648783
Entorhinal	MR-Egger	45.01153	0.2347797
	Inverse variance weighted	46.74919	0.2149053
Frontal pole	MR-Egger	51.17802	0.09164378
	Inverse variance weighted	51.20812	0.11026081
Fusiform	MR-Egger	33.8945	0.7015977
	Inverse variance weighted	35.3841	0.6779649
Inferior parietal	MR-Egger	54.50738	0.05060953
	Inverse variance weighted	54.8379	0.05916865
Inferior temporal	MR-Egger	37.05187	0.559015
	Inverse variance weighted	37.27881	0.593428
Insula	MR-Egger	54.74393	0.04841658
	Inverse variance weighted	56.40161	0.04434429
Isthmus cingulate	MR-Egger	43.8885	0.272001
	Inverse variance weighted	43.92134	0.3089267
Lateral occipital	MR-Egger	66.80433	0.003656039
	Inverse variance weighted	67.05598	0.004675132
Lateral orbitofrontal	MR-Egger	37.63968	0.5319041
	Inverse variance weighted	38.14601	0.5539554
Lingual	MR-Egger	25.74057	0.9492973
	Inverse variance weighted	26.07837	0.9562573
Medial orbitofrontal	MR-Egger	43.73081	0.2775087
	Inverse variance weighted	43.83502	0.3121266
Middle temporal	MR-Egger	35.21808	0.643078
	Inverse variance weighted	36.14967	0.644267
Paracentral	MR-Egger	43.53853	0.2843121
	Inverse variance weighted	44.18875	0.2991325
Parahippocampal	MR-Egger	44.23944	0.2599963
	Inverse variance weighted	44.46003	0.2893824
Pars opercularis	MR-Egger	40.94209	0.3852885
	Inverse variance weighted	43.29363	0.3326096
Pars orbitalis	MR-Egger	46.3846	0.1940741
	Inverse variance weighted	46.82844	0.2125827
Pars triangularis	MR-Egger	54.73514	0.04849656
	Inverse variance weighted	54.99075	0.05755383
Pericalcarine	MR-Egger	40.9379	0.3854638

	Inverse variance weighted	40.97734	0.4274514
Postcentral	MR-Egger	72.35742	0.000925439
	Inverse variance weighted	72.37682	0.001294442
Posterior cingulate	MR-Egger	39.18783	0.4614509
	Inverse variance weighted	39.65309	0.4857295
Precentral	MR-Egger	47.12074	0.1744296
	Inverse variance weighted	47.13811	0.2036735
Precuneus	MR-Egger	39.60568	0.4428657
	Inverse variance weighted	40.03772	0.4685824
Rostral anterior cingulate	MR-Egger	33.30739	0.7265343
	Inverse variance weighted	33.39219	0.760587
Rostral middle frontal	MR-Egger	31.84448	0.7849585
	Inverse variance weighted	32.76124	0.7847206
Superior frontal	MR-Egger	62.21916	0.01047296
	Inverse variance weighted	62.5689	0.0127607
Superior parietal	MR-Egger	38.93501	0.4728037
	Inverse variance weighted	38.9376	0.5179703
Superior temporal	MR-Egger	41.86421	0.3475959
	Inverse variance weighted	44.67028	0.2819567
Supramarginal	MR-Egger	33.2165	0.7303263
	Inverse variance weighted	33.21675	0.7674103
Temporal pole	MR-Egger	39.35957	0.4537835
	Inverse variance weighted	39.423	0.4960549
Transverse temporal	MR-Egger	29.46499	0.86554
	Inverse variance weighted	29.54199	0.8875942

Supplementary Table 6. MR sensitivity analysis of cortical surface area of cerebral functional area in heart failure patients.

Cerebral cortex	Method	Cochran's Q	P
Bankssts	MR-Egger	43.45859	0.2871696
	Inverse variance weighted	44.38683	0.2919947
Caudal anterior cingulate	MR-Egger	55.62494	0.04095567
	Inverse variance weighted	59.78143	0.02287035
Caudal middle frontal	MR-Egger	43.39232	0.2895516
	Inverse variance weighted	44.80686	0.2771945
Cuneus	MR-Egger	50.20767	0.1077826
	Inverse variance weighted	50.20967	0.1292751
Entorhinal	MR-Egger	50.44128	0.1037027
	Inverse variance weighted	50.75089	0.1186733
Frontal pole	MR-Egger	59.94121	0.01713385
	Inverse variance weighted	60.56363	0.01948027
Fusiform	MR-Egger	53.95883	0.05602575
	Inverse variance weighted	55.56295	0.05183819
Inferior parietal	MR-Egger	52.14915	0.07752271
	Inverse variance weighted	53.62679	0.07337278

Inferior temporal	MR-Egger	52.0202	0.07928585
	Inverse variance weighted	52.24359	0.09296391
Insula	MR-Egger	28.86444	0.8826167
	Inverse variance weighted	30.694	0.8549859
Isthmus cingulate	MR-Egger	89.33176	8.04E-06
	Inverse variance weighted	89.92571	1.05E-05
Lateral occipital	MR-Egger	71.9915	0.00101626
	Inverse variance weighted	72.02536	0.001413118
Lateral orbitofrontal	MR-Egger	47.4027	0.1673007
	Inverse variance weighted	47.40452	0.1962198
Lingual	MR-Egger	46.89388	0.1803229
	Inverse variance weighted	46.91982	0.2099263
Medial orbitofrontal	MR-Egger	39.32461	0.4553414
	Inverse variance weighted	39.75916	0.4809858
Middle temporal	MR-Egger	39.46136	0.4492581
	Inverse variance weighted	39.51635	0.4918601
Paracentral	MR-Egger	53.83827	0.05728037
	Inverse variance weighted	53.84188	0.07065973
Parahippocampal	MR-Egger	34.00666	0.6967528
	Inverse variance weighted	35.95928	0.6527204
Pars opercularis	MR-Egger	58.4168	0.02353054
	Inverse variance weighted	58.53463	0.02937326
Pars orbitalis	MR-Egger	39.98337	0.4262844
	Inverse variance weighted	41.14309	0.4203288
Pars triangularis	MR-Egger	40.17411	0.417997
	Inverse variance weighted	41.0692	0.4234989
Pericalcarine	MR-Egger	38.9605	0.4716557
	Inverse variance weighted	38.96237	0.516848
Postcentral	MR-Egger	43.23858	0.2951222
	Inverse variance weighted	43.68739	0.3176415
Posterior cingulate	MR-Egger	98.71798	4.41E-07
	Inverse variance weighted	100.06305	4.70E-07
Precentral	MR-Egger	58.99376	0.0208929
	Inverse variance weighted	61.353	0.01652484
Precuneus	MR-Egger	62.79128	0.009224499
	Inverse variance weighted	63.94157	0.009463078
Rostral anterior cingulate	MR-Egger	63.72689	0.00747466
	Inverse variance weighted	65.11466	0.007286857
Rostral middle frontal	MR-Egger	30.68133	0.8268206
	Inverse variance weighted	31.8421	0.8177259
Superior frontal	MR-Egger	38.32725	0.5003717
	Inverse variance weighted	45.43153	0.2560455
Superior parietal	MR-Egger	36.7003	0.5752397
	Inverse variance weighted	37.00544	0.6058215
Superior temporal	MR-Egger	55.883	0.03896919
	Inverse variance weighted	56.66679	0.04217886

Supramarginal	MR-Egger	31.81319	0.786142
	Inverse variance weighted	31.92403	0.8148943
Temporal pole	MR-Egger	39.5041	0.4473617
	Inverse variance weighted	40.34132	0.4551645
Transverse temporal	MR-Egger	61.30767	0.01278561
	Inverse variance weighted	61.69167	0.01538625
